IN THE UNITED STATES DISTRICT COURT
FOR THE DISTRICT OF DELAWARE

LG DISPLAY CO., LTD., Plaintiff, v. AU OPTRONICS CORPORATION; AU OPTRONICS CORPORATION AMERICA; CHI, MEI OPTOELECTRONICS CORPORATION; and CHI MEI OPTOELECTRONICS USA, INC., Defendants.	C.A. No. 06-726-JJF **CONSOLIDATED CASES**
AU OPTRONICS CORPORATION, Plaintiff, v. LG DISPLAY CO., LTD. and LG DISPLAY AMERICA, INC., Defendants.	C.A. No. 07-357-JJF

SUPPLEMENTAL DECLARATION OF JULIE M. HOLLOWAY IN SUPPORT OF AUO'S RESPONSE TO LGD'S CLAIM CONSTRUCTION BRIEFING ON AUO'S PATENTS

OF COUNSEL:

Vincent K. Yip
Peter J. Wied
Terry D. Garnett
PAUL HASTINGS JANOFSKY & WALKER LLP
515 S. Flower Street, 25th Floor
Los Angeles, CA 90071

Ron E. Shulman
Julie M. Holloway
WILSON SONSINI GOODRICH & ROSATI
650 Page Mill Road
Palo Alto, CA 94304

M. Craig Tyler
Brian D. Range
WILSON SONSINI GOODRICH & ROSATI
8911 Capital of Texas Highway North
Westech 360, Suite 3350
Austin, TX 78759

Richard H. Morse (#531)
John W. Shaw (#3362)
Karen L. Pascale (#2903)
Andrew A. Lundgren (#4429)
YOUNG CONAWAY STARGATT & TAYLOR LLP
The Brandywine Bldg., 17th Floor
1000 West Street
Wilmington, DE 19801
(302) 571-6600

Attorneys for AU Optronics Corporation and AU Optronics Corporation America

September 4, 2008

I, Julie M. Holloway, declare as follows:

1. I, the undersigned, am an member of the law firm of Wilson Sonsini Goodrich & Rosati, P.C., counsel of record for AU Optronics Corporation and AU Optronics Corporation America (collectively, "AUO"). I am an active, licensed member of the State Bar of California and admitted pro hac vice to this Court.

2. Attached hereto as Exhibit 47 is a true and correct copy of an excerpt from the online version of the *Compact Oxford English Dictionary of Current English* (3d ed. 2005), available at www.askoxford.com (last visited Sept. 4, 2008).

3. Attached hereto as Exhibit 48 is the article: Y Hosoya & GW Marshall, Jr., *The Nano-Hardness and Elastic Modulus of Carious and Sound Primary Canine Dentin*, 29-2 Operative Dentistry 142 (2004).

4. Attached hereto as Exhibit 49 is the article: T.A. Kodintseva et al., *Hardness Evaluation of Polytetrafluoroethylene Products*, ECNDT 2006 – Poster 111 (2006).

5. Attached hereto as Exhibit 50 is the article: D. Tabor, *A Simple Theory of Static and Dynamic Hardness* (communicated by Sir Geoffrey Taylor), *in Proceedings of the Royal Society of London: Series A. Mathematical and Physical Sciences* 247 (Vol. 192 1948).

I declare under penalty of perjury under the laws of the United States that the foregoing is true and correct. Executed on September 4, 2008 in Palo Alto, California.

Julie M. Holloway

CERTIFICATE OF SERVICE

I, Karen L. Pascale, Esquire, hereby certify that on September 4, 2008, I caused to be electronically filed a true and correct copy of the foregoing document with the Clerk of the Court using CM/ECF, which will send notification that such filing is available for viewing and downloading to the following counsel of record:

Richard D. Kirk [rkirk@bayardfirm.com]
Ashley B. Stitzer [astitzer@bayardfirm.com]
BAYARD, P.A.
222 Delaware Avenue, Suite 900
P.O. Box. 25130
Wilmington, DE 19899-5130
(302) 655-5000
Attorneys for LG Display Co., Ltd. and LG Display America, Inc.

Philip A. Rovner [provner@potteranderson.com]
David E. Moore [dmoore@potteranderson.com]
POTTER, ANDERSON & CORROON
6th Floor, Hercules Plaza
1313 N. Market Street
Wilmington, DE 19801
Attorneys for Chi Mei Optoelectronics Corporation and Chi Mei Optoelectronics USA, Inc.

I further certify that I caused a copy of the foregoing document to be served by e-mail on the above-listed counsel of record and on the following non-registered participants in the manner indicated:

By E-mail

Gaspare J. Bono [gbono@mckennalong.com]
Matthew T. Bailey [mbailey@mckennalong.com]
R. Tyler Goodwyn, IV [tgoodwyn@mckennalong.com]
Lora A. Brzezynski [lbrzezynski@mckennalong.com]
Cass W. Christenson [cchristenson@mckennalong.com]
MCKENNA LONG & ALDRIDGE LLP
1900 K Street, NW
Washington, DC 20006
(202) 496-7500
Attorneys for LG Display Co., Ltd. and LG Display America, Inc.

Jonathan S. Kagan [jkagan@irell.com]
Alexander C.D. Giza [agiza@irell.com]
IRELL & MANELLA LLP
1800 Avenue of the Stars
Suite 900
Los Angeles, CA 90067
(310) 277-1010
Attorneys for Chi Mei Optoelectronics Corporation and Chi Mei Optoelectronics USA, Inc.

YOUNG CONAWAY STARGATT & TAYLOR LLP

/s/ Karen L. Pascale

September 4, 2008

Richard H. Morse (#531) *[rmorse@ycst.com]*
John W. Shaw (#3362) *[jshaw@ycst.com]*
Karen L. Pascale (#2903) *[kpascale@ycst.com]*
Andrew A. Lundgren (#4429) [*alundgren@ycst.com]*
The Brandywine Building
1000 West St., 17th Floor
P.O. Box 391
Wilmington, Delaware 19899-0391
Phone: 302-571-6600
Attorneys for AU Optronics Corporation and AU Optronics Corporation America

Exhibit 47

Compact Oxford English Dictionary

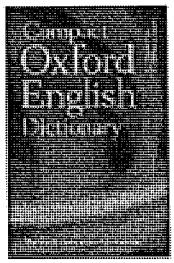

form

• **noun 1** visible shape or configuration. **2** a way in which a thing exists or appears. **3** a type or variety. **4** the customary or correct method or procedure. **5** a printed document with blank spaces for information to be inserted. **6** chiefly Brit. a class or year in a school. **7** the state of a sports player with regard to their current standard of play. **8** details of previous performances by a racehorse or greyhound. **9** a person's mood and state of health: *she was on good form.* Brit. a long bench without a back.

• **verb 1** bring together parts to create. **2** go to make up. **3** establish or develop. **4** make or be made into a certain form.

— PHRASES **in** (or Brit. **on**) **form** playing or performing well. **off** (or Brit. **out of**) **form** not playing or performing well.

— DERIVATIVES **formable** adjective **formless** adjective.

— ORIGIN Latin *forma* 'a mould or form'.

Perform another search of the Compact Oxford English Dictionary

About this dictionary
The *Compact Oxford English Dictionary of Current English* contains 145,000 words, phrases, and definitions.
Find out more about Oxford's range of English dictionaries
Sign up for the AskOxford Word of the Day

Search the Little Oxford Dictionary of Quotations
Search the Concise Dictionary of First Names

- Ask The Experts
- Better Writing
- World of Words
- Games
- Global English
- Foreign Languages

LINKS

- AskOxford Shop
- External Web Links
- OUP Website
- Children's Dictionaries
- ELT Dictionaries
- Oxford Online

OXFORD UNIVERSITY PRESS

Exhibit 48

©Operative Dentistry, 2004, **29-2,** 142-149

Laboratory Research

The Nano-Hardness and Elastic Modulus of Carious and Sound Primary Canine Dentin

Y Hosoya • GW Marshall, Jr

Clinical Relevance

The significantly lower nanohardness and elasticity of dentin under the lesion near the pulp and cervical area might have a deleterious effect on resin adhesion.

SUMMARY

This study measured the nanohardness and elastic modulus of carious and sound primary canine dentin and compared the values obtained under the lesion and in sound regions of incisal, center and cervical areas, and outer, middle and inner layers. Six extracted or exfoliated primary canines (three with dentin caries on both proximal surfaces and three that were sound teeth) were mesio-distally sectioned parallel to the long axis of the tooth and polished. The hardness (H), plastic hardness (PH) and Young's modulus (Y) were measured by a nano-indentation tester. Ten indentations at intervals of 10 μm on all regions, areas and layers were made using a load of 1 gf for one second. All indentations were observed using a microscope attached to the tester. All data was statistically analyzed using ANOVA and Scheffe's test at $p<0.05$. For sound teeth, the H, PH and Y values of the inner layer were significantly lower than the outer and middle layers in all areas. The H, PH and Y values of the cervical area were significantly lower than the incisal area in almost all of the outer, middle and inner layers. For carious teeth, the H, PH and Y values of the inner layer were significantly lower than the outer and middle layers in the center area. For the center area, the H, PH and Y values under the lesion were significantly lower than sound teeth in the outer and middle layers. Dentin under the lesion, near the pulp and cervical areas showed significantly lower nanohardness and elasticity.

*Yumiko Hosoya, DDS, PhD, associate professor, Division of Pediatric Dentistry, Department of Developmental and Reconstructive Medicine, Course of Medical and Dental Sciences, Nagasaki University Graduate School of Biomedical Sciences, Nagasaki, Japan

Grayson W Marshall, Jr, DDS, MPH, PhD, professor, Division of Biomaterials and Bioengineering, Department of Preventive and Restorative Dental Science, University of California San Francisco, San Francisco, CA, USA

*Reprint request: 1-7-1, Sakamoto, Nagasaki, 852-8588, Japan; e-mail: hosoya@net.nagasaki-u.ac.jp

INTRODUCTION

Improved resin bonding yields strong bonds to enamel with excellent sealing ability (Retief, 1987). However, the resin-dentin seal is much less reliable. Caries modifies the structure and typical carious lesions contain various zones of the affected layer (Fusayama, Okuse & Hosoda, 1966) that have varying mineral levels and properties. Fusayama (1993) compared the structure and characteristics of three layers of dentin of carious teeth (outer caries dentin, inner carious dentin and normal dentin). Outer caries dentin or the discolored layer

is infected and unremineralizable and should be removed for carious treatment. Inner carious dentin is classified into turbid, transparent and subtransparent layers. These layers are uninfected and remineralizable and should be preserved for caries treatment. Similar zones have been observed in primary teeth with carious lesions (Hosoya & others, 2000; Hosoya, Ono & Marshall, 2002), but only limited work has been done to define the properties of these altered zones. Although permanent tooth dentin has been studied extensively, the microstructure of dentin in primary teeth has received only limited attention. A better understanding of dentin in primary teeth, especially carious primary dentin, is needed to improve dentin bonding methods and make dental restorations more effective and successful.

The hardness and elasticity of fully mineralized permanent dentin have been reported in numerous studies (Craig, Gehring & Peyton, 1958; Bowen & Rodriguez, 1962; Fusayama & Maeda, 1969; Pashley, Okabe & Parham, 1985; Sano & others, 1994; Kinney & others, 1996; Urabe & others, 2000; Mahoney & others, 2000). Recently, nano-indentation has been used to measure hardness and Young's modulus of dentin on a submicroscopic scale (Urabe & others, 2000; Mahoney & others, 2000). The range in hardness of sound permanent dentin is broad, from 0.2-0.8 GPa (1MPa=10.2 kgf/cm^2, 1GPa=101.93675 kgf/mm^2) (Fusayama & Maeda, 1969; Pashley & others, 1985; Sano & others, 1994; Kinney & others, 1996). Young's modulus of sound permanent dentin ranged from about 10 – 20 GPa (Craig & Peyton, 1958; Bowen & Rodriguez, 1962; Lehmann, 1967; Sano & others, 1994; Kinney & others, 1996; Meredith & others, 1996; Xu & others, 1998; Kinney & others, 1999). Few studies of the hardness of primary dentin have been reported (Johnsen, 1994; Mahoney & others, 2000; Hosoya & others, 2000; Hosoya & others, 2002) and Knoop hardness values for sound primary dentin ranged from 35 to 60 KHN (Johnsen, 1994) depending on location within the tooth.

Fusayama and others (1966) and Ogawa and others (1983) reported the Knoop hardness of carious permanent dentin for discolored, transparent and subtransparent layers and sound dentin and found that all zones, including the transparent zone of the affected layer, were softer than normal dentin. Craig, Gehring and Peyton (1959) also measured the hardness of carious permanent dentin but reported that some zones were harder than normal dentin.

Hosoya and others (2000; 2002) measured the Knoop hardness of carious primary anterior tooth dentin in caries-affected layers including transparent dentin, adjacent sound dentin and dentin regions far from and not related to caries. The results of these reports (Hosoya & others, 2000; Hosoya & others, 2002) showed that primary dentin in areas under lesions and in adjacent regions on the carious side of the teeth had significantly lower hardness than corresponding areas on the sound side. Under the lesion, significantly lower Knoop hardness values were obtained in the region less than 150 μm from the bottom of the cavity and the Ca and P contents at depths less than 100 μm from the bottom of cavity were significantly lower than those at greater distance (Hosoya & others, 2002). Transparent dentin was softer than sound dentin (Hosoya & others, 2000; Hosoya & others, 2002). The reduced mechanical properties of the affected layers of carious dentin suggest that bonding to this weakened structure may be more difficult. This has been reported by several workers for permanent dentin (Nakajima & others, 1995; Nakajima & others, 1999).

The elastic properties of dentin are important for understanding the mechanical properties of calcified tissue and for alterations in the mechanical response due to caries, sclerosis and aging, as well as understanding the effects of adhesive materials to dentin. Mahoney and others (2000) measured the hardness and elastic modulus of sound maxillary primary molar dentin using a nano-indentation tester. However, they used not only sound teeth but also carious teeth as sample teeth and calculated the mixed data. They did not compare the values at different depths or locations of dentin. The elasticity of carious dentin has not been reported for primary carious teeth and only limited studies have been reported for permanent teeth (Marshall & others, 2001).

This study measured the nanohardness and elastic modulus of carious and sound canine dentin and compared the values among areas under the lesions and in sound regions of the incisal, center and cervical areas in the outer, middle and inner layers of each area.

METHODS AND MATERIALS

Sample Teeth

Three sound maxillary primary canines and three mandibular primary canines with caries at the center portion of both proximal surfaces were used for this study. All teeth were extracted or exfoliated by eruption of the succedaneous permanent tooth or extracted as required for orthodontic treatment from Japanese children. The teeth were stored in 4°C physiologic saline solution shortly after extraction or exfoliation. The age of the patients ranged from six years four months to seven years nine months. Informed consent was obtained from the parents and patients in order to collect the teeth. Radiographs were taken to identify the carious areas. The total number of carious lesions was six. In all carious lesions, caries did not extend more than one-fourth the depth of the dentin.

Specimen Preparation

Sound teeth were mesiodistally sectioned parallel to the long axis at the center of the tooth. For carious teeth

with caries on both proximal surfaces, the teeth were longitudinally sectioned through the central part of the largest carious lesion. Sectioning was done using a low-speed saw (Buehler Ltd, Lake Bluff, IL, USA) with a circular diamond blade and copious filtered water.

After sectioning, the specimens were polished on wet silicon carbide paper using grit sizes of 600, 800, 1000 and 1200. Final polishing was carried out on felt cloth using 3, 1, 0.1, 0.3 and 0.05 µm-size aluminum oxide suspensions (Baikowski International Co, Charlotte, NC, USA). Optical photomicrographs of the polished specimens were taken with a microscope (Olympus Co, Tokyo, Japan), and the infected, affected and sound portions of the dentin were identified. The sectioned and polished specimens were stored in 4°C distilled water until measurement and were dried at room temperature for 20 minutes prior to the study.

Nano-Indentation Test

Cyanoacrylate (Konishi Co, Tokyo, Japan) was applied onto small areas of enamel of the specimen, and the specimen was then fixed on a flat glass plate to stabilize its surface and orient the surface parallel to the stage of the nano-indentation tester ENT-1100 (Elionix Co, Tokyo, Japan). ENT-1100 is a depth sensing computer-controlled instrument and has a Berkovich indentor, a three-sided pyramid diamond probe. The instrument was enclosed in an isolation chamber with a temperature controller and placed on an ALD anti-vibration isolator in order to minimize influences of environmental conditions such as room temperature, floor-vibration and noise. The specimen was kept in dry conditions during measurement since this machine can control temperature in the chamber at 26°C but not humidity. The loading control system was powered by electromagnetic force and load ranges from 10 mgf to 100 gf. The position of indentation could be programmed and the indents observed with a CCD camera attached to the tester.

Figure 1 shows a load vs displacement curve from the measurement process. Values of hardness (H), plastic hardness (PH) and Young's modulus (Y) were calculated according to the equations (1), (2) and (3), respectively, following the index of Elionix company that was modified from the method reported by Oliver and Pharr (1992):

$$H=3.7926 \times 10^{-2} \times P_{max}/h_{max}^2 \quad (1)$$

$$PH=3.7926 \times 10^{-2} \times P_{max}/h_1^2 \quad (2)$$

$$Y=1.81092 \times 10^{-3} \times 1/h_1 \times dp/dh \quad (3)$$

in which P_{max} is the maximum applied load, h_{max} is the maximum penetration depth, h_1 is the intercept depth and dP/dh is the contact stiffness from the unloading portion of the load vs displacement curve.

Figure 2 shows the names of the areas and layers of the sample teeth for measurement. For sound teeth, the mesial and distal sides were divided into incisal, center and cervical areas, and for the carious teeth, the mesial and distal sides were divided into center and mesial incisal areas. Distal incisal areas were not measured because the small size of the teeth relative to the lesion size suggested that this area would have been altered by caries. The cervical area of the carious teeth was not measured in this study, because this area could not be reliably measured in the carious teeth due to the presence of caries. Then, each area was divided into outer, middle and inner layers. For regions under the lesion, the term "under the lesion" was used instead of the term "outer layer."

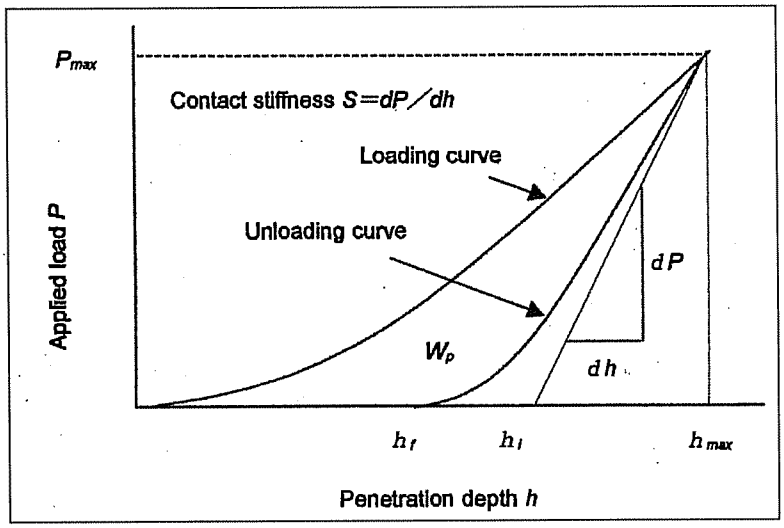

Figure 1. *Load vs displacement curve in the measurement process.*

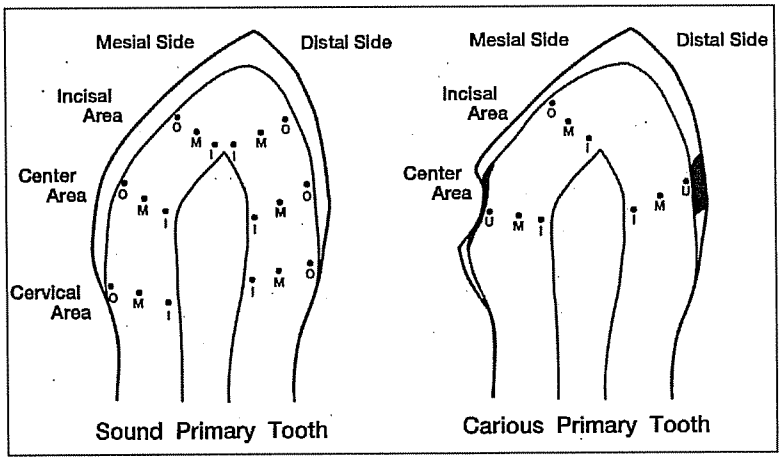

Figure 2. *Names of the areas and layers of the sample teeth in measurement (O: outer layer, M: middle layer, I: inner layer, U: under the lesion layer).*

Ten indentations at intervals of 10 μm in each of the subdivided regions were made perpendicular to the outline of the dentinoenamel junction or DEJ using a load of 1 gf for one second. The positions of the indentations were as follows. The first point of the outer layer was made at 10 μm beneath the DEJ. The first point of the middle layer was made at the center from the DEJ to the pulp chamber wall. The last point of the inner layer was made at the most inner measuring point in primary dentin close to the pulp chamber wall. Indentations were observed using a microscope with a CCD camera attached to the tester under 700x magnification. Some of the indentations were also observed using a scanning electron microscope (SEM) S-3500 (Hitachi Ltd, Tokyo, Japan). For regions under the lesion, measurement was started just internal to the infected and destroyed dentin layer, and the shape of the indentation at the first point was verified by examining the indents with the CCD camera and SEM. Irregular or unclear shaped indentations were removed from the data. Therefore, all of the selected indentations were marked on the intertubular dentin.

All data was statistically analyzed using ANOVA followed by Scheffe's multiple comparison testing and correlation coefficients at $p<0.05$.

RESULTS

First, the means and standard deviations of the values of 10 indentations on each layer were calculated and compared to different areas and layers on the same sample. Tooth to tooth differences existed but regional differences were similar on all samples. Then, the values for all samples were mixed and statistically compared among different areas and layers in this study.

Table 1 shows the hardness, plastic hardness and Young's modulus of sound primary canine dentin. In general, related to the incisal, center and cervical areas, the hardness, plastic hardness and Young's modulus decreased from DEJ to pulp and the values of the inner layer were significantly lower than the outer and middle layers. For cervical areas, the hardness and plastic hardness of the outer layer were significantly higher than the middle and inner layers. Comparing values in the same layer among the different areas, the hardness, plastic hardness and Young's modulus were reduced from incisal to cervical areas and, in general, the values of the cervical area were significantly lower than those of the incisal and center areas.

Table 2 shows the hardness, plastic hardness and Young's modulus of carious primary canine dentin. For the center area or under the decayed area, all values of the inner layer were significantly lower than the outer and middle layers. In the incisal area, which was a sound region of the carious teeth, the values of the outer layer were significantly higher than the middle and inner layers.

Table 3 compares the hardness, plastic hardness and Young's modulus of carious primary canine dentin and sound primary canine dentin. The center area had values under the lesion that were significantly lower than the sound teeth in the outer and middle layers.

Two- or three-way ANOVA and Scheffe's tests indicated that the depth of dentin and caries decay had the most significant influence on the values, and the area of dentin also had a second significant influence on the values.

Figures 3 and 4 show the average hardness and Young's modulus, respectively, for sound and carious primary canine dentin on both the mesial and distal sides of the teeth. The trends for both were similar.

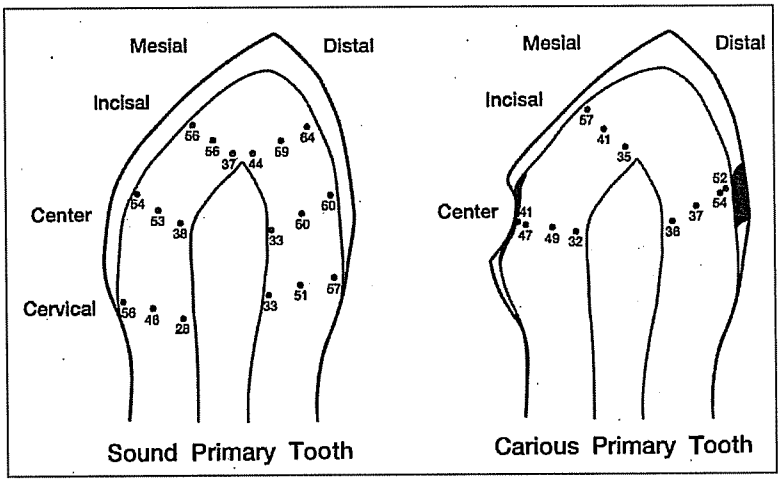

Figure 3. *Average hardness values of sound and carious primary canine dentin.*

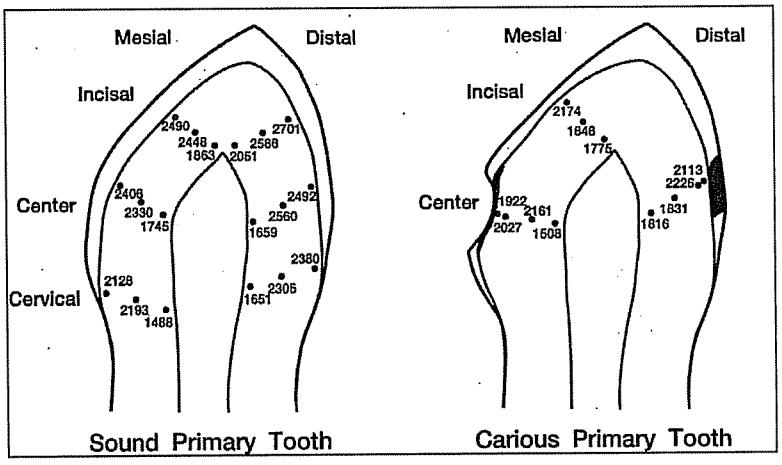

Figure 4. *Average Young's modulus of sound and carious primary canine dentin.*

Table 1: *Hardness, Plastic Hardness and Young's Modulus of Sound Primary Canine Dentin (unit: kgf/mm²)*

Area	Layer	Hardness Mean (SD)	Plastic Hardness Mean (SD)	Young's Modulus Mean (SD)	Number of Measurements
Incisal	Outer	60.0 (8.0)	71.5 (12.6)	2597 (367)	59
	Middle	57.3 (13.9)	74.3 (19.7)	2517 (423)	60
	Inner	40.6 (10.7)	50.6 (14.8)	1957 (364)	60
Center	Outer	57.0 (11.3)	71.6 (15.8)	2447 (393)	60
	Middle	56.8 (12.6)	71.6 (18.0)	2445 (379)	58
	Inner	35.4 (10.4)	44.3 (14.5)	1702 (347)	60
Cervical	Outer	56.8 (6.7)	76.5 (11.7)	2254 (341)	60
	Middle	48.7 (12.4)	60.8 (18.8)	2249 (312)	60
	Inner	30.6 (9.4)	36.6 (13.4)	1569 (263)	60

Vertical line: no significant difference at p<0.05

Table 2: *Hardness, Plastic Hardness and Young's Modulus of Carious Primary Dentin (unit: kgf/mm²)*

Area	Layer	Hardness Mean (SD)	Plastic Hardness Mean (SD)	Young's Modulus Mean (SD)	Number of Measurements
Center	Under Lesion	46.9 (19.5)	57.5 (25.0)	2023(618)	59
	Middle	42.9 (17.7)	53.5 (23.5)	1996 (700)	60
	Inner	33.6 (12.0)	41.0 (15.8)	1662 (498)	60
Incisal	Outer	57.1 (15.1)	77.2 (20.7)	2174 (593)	29
	Middle	40.7 (21.0)	52.0 (30.2)	1846 (596)	30
	Inner	34.8 (11.2)	42.0 (14.7)	1775 (429)	30

Vertical line: no signilicant difference at p<0.05

Table 3: *Hardness, Plastic Hardness, and Young's Modulus of Carious and Sound Primay Dentin (unit: kgf/mm²)*

Layer	Tooth	Area	Hardness Mean (SD)	Plastic Hardness Mean (SD)	Young's Modulus Mean (SD)	Number of Measurements
Under Lesion	Carious	Center	46.9 (19.5)	57.5 (25.0)	2023 (618)	59
Outer	Carious	Incisal	57.1 (15.1)	77.2 (20.7)	2174 (593)	29
Outer	Sound	Center	57.0 (11.3)	71.6 (15.8)	2447 (393)	60
Middle	Carious	Center	42.9 (17.7)	53.5 (23.5)	1996 (700)	60
Middle	Carious	Incisal	40.7 (21.0)	52.0 (30.2)	1846 (596)	30
Middle	Sound	Center	56.8 (12.6)	71.6 (18.0)	2445 (379)	58
Inner	Carious	Center	33.6 (12.0)	41.0 (15.8)	1662 (498)	60
Inner	Carious	Incisal	34.8 (11.2)	42.0 (14.7)	1776 (429)	30
Inner	Sound	Center	35.4 (10.4)	44.3 (14.5)	1702 (347)	60

Vertical line: no significant difference at p<0.05

Under the lesion, not only the average values but also the values at the first measuring point located in the discolored layer were plotted on the figures. Values under the lesion and in the middle layers under the decayed areas or center area of the carious teeth were significantly lower than either the outer or middle layers at the center areas in the sound teeth.

Hardness and Young's modulus showed significant correlations (corr = 0.932, $p<0.0001$).

DISCUSSION

The nano-indentation technique has several advantages for determining hardness over conventional microhardness methods such as Vickers and Knoop hardness. This technique has the ability to produce small indentations under small loads and can measure both the hardness and elastic modulus of materials. Previous reports have suggested wide variations in the basic mechanical properties of dentin. Some of this variation may result from using techniques such as microhardness, which yield averaged values that include contributions from the tubules, peritubular dentin and intertubular dentin. Since the quality of each dentin component might vary with location, this could contribute to the wide range of values. However, work by Kinney and others (1996) indicated that much

of the variation in permanent teeth could result from differences in intertubular dentin rather than peritubular dentin. In this work, we used a nanoindentation technique that allowed measurement of the intertubular dentin alone.

Sound Teeth

In this study, the hardness values of sound primary canine dentin ranged from 30 to 60 kgf/mm² and plastic hardness ranged from 37 to 77 kgf/mm² (Table 1, Figure 3). These values were lower than that for primary molars (0.92 GPa or 94 kgf/mm²) as reported by Mahoney and others (2000) but were in agreement with previous studies of sound permanent dentin (Fusayama & Maeda, 1969; Pashley & others, 1985; Sano & others, 1994; Kinney & others, 1996). Hardness is calculated by maximum penetration depth that includes both plastic and elastic deformation of dentin. Plastic hardness is calculated based only on the plastic deformation of dentin and corresponds to Vicker's hardness. In this study, variations in hardness and plastic hardness were almost the same for all layers and areas. Young's modulus of dentin for sound primary canines ranged from about 1600 to 2600 kgf/mm² (Table 1, Figure 4). These values were in agreement with a previous study of primary molar dentin (19.89 GPa or 2029 kgf/mm2) (Mahoney & others, 2000) and sound permanent dentin (Craig & Peyton, 1958; Bowen & Rodriguez, 1962; Lehmann, 1967; Sano & others, 1994; Kinney & others, 1996; Meredith & others, 1996; Xu & others, 1998; Kinney & others, 1999).

No report using a nano-indentation technique has compared the hardness and elasticity among the depths and areas of primary dentin. Meredith and others (1996) and Hosoya and others (2000; 2002) reported that the hardness of dentin decreased with distance from the dentinoenamel junction, while Pashley and others (1985) reported a highly significant inverse correlation in permanent dentin between dentin microhardness and tubule numerical density that increases with depth. However, Kinney and others (1996) reported that most of the decrease in dentin hardness upon approaching the pulp chamber could be attributed to changes in the hardness of intertubular dentin, not just the increase in the number of tubules.

In this study, for all areas, hardness, plastic hardness and Young's modulus of the inner layer were significantly lower than that of the outer and middle layers (Table 1). These results for the hardness and plastic hardness agreed with previous studies (Craig & Peyton, 1958; Bowen & Rodriguez, 1962; Lehmann, 1967; Sano & others, 1994; Kinney & others, 1996; Meredith & others, 1996; Kinney & others, 1999), but the result of the Young's modulus was in disagreement with suggestions by Kinney and others (1999). They utilized atomic-force microscope (AFM) based nanoindentation measurements and suggested that Young's modulus was dominated by the properties of intertubular dentin and could show a slight increase from outer to inner dentin. However, the current study showed significant correlations among the values of hardness and Young's modulus, which were in agreement with the previous report for primary molars (Mahoney & others, 2000).

In this study, there was no significant difference in hardness, plastic hardness and Young's modulus between the outer and middle layers of all areas, except for the hardness and plastic hardness of the cervical area. Since the outer layer of this study was positioned 10-110 μm beneath the DEJ, the finding that there was no significant hardness difference between the outer and middle layers might be due to the influence of the mantle dentin.

Carious Teeth

Craig and others (1959) reported that permanent dentin surrounding a caries lesion had a hardness of 10 KHN greater than sound dentin; the hardness at the center of the lesion was significantly lower and transparent dentin was 10 KHN harder than the adjacent area. Fusayama and others (1966) and Ogawa and others (1983) reported that Knoop hardness for the discolored layer of carious permanent dentin ranged from 20 to 27 KHN, the transparent layer from 27 to 48 KHN, the subtransparent layer from 48 to 68 KHN, and sound dentin varied from 21 to 68 KHN. In our previous study (Hosoya & others, 2002), the average Knoop hardness values of primary canine dentin under the lesion ranged from 31 to 43 KHN in the outer layer, 35 to 44 KHN in the middle layer and 30 to 43 KHN in the inner layer, respectively. However, values less than 150 μm from the bottom of cavity were about 29 KHN and were lower than the region 250 μm away from the cavity. The hardness of many layers and areas of the carious side of carious primary canines, even in apparently unaffected dentin, were significantly lower than the sound side of carious primary canines, suggesting that they were affected by caries. In our previous study on carious primary anterior teeth (Hosoya & others, 2000), the transparent layer had significantly higher hardness than the more superficial decayed layer, but it was not significantly different from adjacent areas or areas to the side of the lesion. In another previous study (Hosoya & others, 2002), there was no significant difference in hardness between transparent dentin and non-transparent dentin in the same areas and layers. Marshall and others (2001) reported that the hardness and elastic modulus of intertubular dentin decreased slightly or was unchanged in the transparent dentin of permanent teeth.

In the incisal area that was sound in carious teeth, the hardness, plastic hardness and Young's modulus of

the outer layer were significantly higher than the middle and inner layers. However, in the center area that was under the decayed area, there was no significant difference in hardness, plastic hardness and Young's modulus under the lesion (outer) and middle layers (Table 2). All mechanical values under the lesion were significantly lower than the corresponding regions of sound teeth (Table 3), although caries did not extend more than one-fourth the depth of the dentin in the teeth used for this study. Therefore, the results of this study indicate that not only in the obviously affected layer but also in the areas adjacent to the lesion not obviously affected by caries, the dentin was softer and had a lower elastic modulus than sound dentin (Figures 3 and 4). In this study, the lesions were small and only one linear measurement was done under the carious area. Therefore, the values of the transparent dentin could not be statistically analyzed. However, no significant difference was obtained between the values of the first measuring point under the lesion, which was positioned 10 μm from the bottom of cavity and the discolored dentin and the average values under the lesion, which included all measurements 10-110 μm from the bottom of cavity and included not only discolored dentin but also transparent dentin (Figures 3 and 4). This further suggests that transparent dentin may not be sclerotic as noted by other studies (Fusayama & others, 1966; Ogawa and others, 1983; Hosoya and others, 2000; Marshall and others, 2001).

The results of this study showed that hardness and elastic modulus of dentin differed with intratooth location and decreased with distance from the DEJ in primary canine dentin (Tables 1-3, Figures 3 and 4). Hardness and elastic modulus of dentin might also differ with tooth type and environmental factors during the time of tooth formation and mineralization. In this study, all the sound teeth were maxillary primary canines but all the carious teeth were mandibular primary canines. In addition, the position of the carious lesion was almost at the center area of the proximal surfaces but was not the same among the specimens. The depth from the DEJ to the first measuring point under the lesion differed among the carious teeth and differed between the sound and carious teeth. These differences, due to varying lesion shapes, caused considerable variation among the specimens but, in general, both dentin under the lesion and apparently normal dentin adjacent to the lesion had reduced hardness and elastic modulus compared to sound dentin. None of the areas associated with carious teeth had increased values, thus, there was no evidence of sclerotic dentin in these lesions.

Although the use of nano-indentation permits smaller areas than microhardness to be measured, both the microhardness and nano-indentation equipment used for this study were carried out on dried tissues. When demineralized dentin is dried, it collapses (Marshall & others, 1998), and indentations on the collapsed layer could be influenced by the underlying mineralized tissue. Improved methods such as an AFM-based indentation, which allows submicroscopic indentations of hydrated tissues, may be needed to improve accuracy of the values of various altered layers of carious dentin (Balooch & others, 1998; Marshall and others, 2001).

This study and our previous work (Hosoya & others, 2000; Hosoya & others, 2002) indicate that lower hardness and elastic modulus values were obtained under the caries region and also in the region adjacent to the caries that was apparently not affected by the lesion. This could have a deleterious effect on resin adhesion to these regions. After etching, the hardness might be lower or the depth of demineralization might be increased so that bonding to these areas might require specific etching treatments that have not yet been defined. Previous reports (Nor & others, 1997; Olmez & others, 1998; Hosoya & others, 2001) suggested that primary dentin is more susceptible to acid or some chemical conditioning treatments and, therefore, shorter application times for the dentin conditioner in primary dentin may be appropriate. Further study is required to understand the precise mechanism of adhesion between carious dentin and resinous materials and whether different treatments are needed to optimize bonding for primary and permanent dentin.

CONCLUSIONS

1. Hardness and elastic modulus of sound primary canine dentin were consistent with prior reported results for permanent dentin.
2. Hardness and elastic modulus for primary canine teeth with carious lesions showed markedly lower mechanical properties than sound primary dentin. No areas with increased mechanical properties were observed, thus, there was no evidence of sclerotic dentin associated with primary canine caries.
3. Apparently unaffected dentin in areas adjacent to carious lesions had reduced mechanical properties compared to primary dentin in sound teeth.

Acknowledgements

The authors acknowledge Mr Hideo Suzuki and Mr Takahiko Uematsu (Elionix Co) for their technical assistance in the operation of the nanoindentation tester. This study was partially supported by the Japanese Ministry of Education, Science, Sport and Culture grant 11672053 and 14571955.

(Received 30 January 2003)

References

Balooch M, Wu-Magidi IC, Lundkvist AS, Marshall SJ, Marshall GW, Seikhaus WJ & Kinney JH (1998) Viscoelastic properties of demineralized human dentin in water with AFM-based indentation *Journal of Biomedical Materials Research* **40** 539-544.

Bowen RL & Rodriguez MM (1962) Tensile and modulus of elasticity of tooth structure and several restorative materials *Journal of the American Dental Association* **64** 378-387.

Craig RG & Peyton FA (1958) Elastic and mechanical properties of human dentin *Journal of Dental Research* **37** 710-718.

Craig RG, Gehring PE & Peyton FA (1959) Relation of structure to the microhardness of human dentin *Journal of Dental Research* **38** 624-630.

Fusayama T, Okuse K & Hosoda H (1966) Relationship between hardness, discoloration, and microbial invasion in caries dentin *Journal of Dental Research* **45** 1033-1046.

Fusayama T & Maeda T (1969) Effect of pulpectomy on dentin hardness *Journal of Dental Research* **48** 452-460.

Fusayama T (1993) New concepts in the pathology and treatment of dental caries A simple pain-free adhesive restorative system by minimal reduction and total etching Ishiyaku Euro America Inc, St Louis, MO p 1-16.

Hosoya Y, Marshall SJ, Watanabe LG & Marshall GW (2000) Microhardness of carious deciduous dentin *Operative Dentistry* **25(1)** 81-89.

Hosoya Y, Kawashita Y, Marshall GW Jr & Goto G (2001) Influence of Carisolv™ for resin adhesion to sound human primary dentin and young permanent dentin *Journal Dentistry* **29** 163-171.

Hosoya Y, Ono T & Marshall GW (2002) Microhardness of carious primary canine dentin *Pediatric Dentistry Journal* **12** 91-98.

Johnsen DV (1994) Comparison of Primary and Permanent Teeth Oral Development and Histology 2nd ed JK Avery, New York: Thiema Medical Publishers p 287.

Kinney JH, Balooch M, Marshall SJ, Marshall GW Jr & Weihs TP (1996) Hardness and Young's modulus of human peritubuler and intertubular dentin *Archives of Oral Biology* **4** 9-13.

Kinney JH, Balooch M, Marshall GW & Marshall SJ (1999) A micromechanics model of the elastic properties of human dentin *Archives of Oral Biology* **44** 813-822.

Lehmann M (1967) Tensile strength of human dentin *Journal of Dental Research* **46** 197-201.

Mahoney E, Holt A, Swain M & Kilpatrik N (2000) The hardness and modulus of elasticity of primary molar teeth: An ultra-micro-indentation study *Journal of Dentistry* **28** 589-594.

Marshall GW, Wu-Magidi IC, Watanabe LG, Inai N, Balooch M & Kinney SJ (1998) Effect of citric acid concentration on dentin demineralization, dehydration and rehydration: An AFM study *Journal of Biomedical Materials Research* **42** 500-507.

Marshall GW, Habelitz S, Gallagher R, Balooch M & Marshall SJ (2001) Nanomechanical properties of hydrated caries human dentin *Journal Dental Research* **80** 1768-1771.

Meredith N, Sherriff M, Stechell DJ & Swanson SA (1996) Measurement of the microhardness and Young's modulus of human enamel and dentine using an indentation technique *Archives of Oral Biology* **41** 539-545.

Nakajima M, Sano H, Burrow MF, Tagami J, Yoshiyama E, Ebisu S, Ciucchi B, Russell CM & Pashley DH (1995) Tensile bond strength and SEM evaluation of caries-affected dentin using dentin adhesives *Journal of Dental Research* **74** 1679-1688.

Nakajima M, Ogata M, Okuda M, Tagami J, Sano H & Pashley DH (1999) Bonding to caries-affected dentin using self-etching primers *American Journal of Dentistry* **12** 309-314.

Nor JE, Feigel RJ, Dennison JB & Edward CA (1997) Dentin bonding: SEM comparison of the dentin surface in primary and permanent teeth *Pediatric Dentistry* **19** 246-252.

Ogawa K, Yamashita Y, Ichijo T & Fusayama T (1983) The ultrastructure and hardness of the transparent layer of human carious dentin *Journal of Dental Research* **62** 7-10.

Olmez A, Oztas N, Basak F & Erdal S (1998) Comparison of the resin-dentin interface in primary and permanent teeth *Journal of Clinical Pediatric Dentistry* **22** 293-298.

Oliver WC, Pharr GW (1992) An improved technique for determining hardness and elastic modulus using load and displacement sensing indentation experiments *Journal of Materials Research* **7** 1564-1583.

Pashley DH, Okabe A & Parham P (1985) The relationship between dentin microhardness and tubule density *Endo Dental Traumatology* **1** 176-179.

Retief DH (1987) Are adhesive techniques sufficient to prevent microleakage? *Operative Dentistry* **12** 140-145.

Sano H, Ciucchi B, Matthews WG & Pashley DH (1994) Tensile properties of mineralized and demineralized human and bovine dentin *Journal of Dental Research* **73** 1205-1211.

Urabe I, Nakajima M, Sano H & Tgami J (2000) Physical properties of the dentin-enamel junction region *American Journal of Dentistry* **13** 129-135.

Exhibit 49

Hardness Evaluation of Polytetrafluoroethylene Products

T.A.KODINTSEVA, A.M.KASHKAROV, V.A.KALOSHIN NPO Energomash Khimky, Russia
A.P.KREN, V.A.RUDNITSKY, Institute of Applied Physics of the National Academy of Sciences of Belarus, Minsk, Belarus

Abstract. Influence of the strain rate on process of hardness measurement of teflon (PTFE) products by impact indentation method is considered. Possibility of hardness measurement at given value of intrusion depth is shown. Expression for coefficient of dynamics, taking account of influence of strain rate on results of hardness measurement is presented.

The goal of this paper is to consider the possibility of application of the dynamic indentation test method for the investigation of polytetrafluoroethelene materials (or PTFE), service properties of which depend on chemical composition and regime of heat treatment. It is known that among different test methods the most suitable ones for the evaluation of the properties of polymeric materials are indentation methods. In accordance with loading velocity indentation methods can be static or dynamic ones. Dynamic methods has number of advantages, the main of them are high test productivity and wide range of using. Moreover devices, based on these methods are small-sized and very convenient for using, because of the impact loading makes possible to produce rather high contact forces at small displacements. The last statement allows to consider impact dynamic devices as non-destructive ones and because of they can use for testing of finishing products.
Taking into account that the working pressure in PTFE products must to be no more than yield stress, the main parameters to be tested are hardness and yield stress of the material.
Hardness of PTFE in accordance with ISO 2039/1 is determined as the ratio of the maximum load P_{max} acting on the indenter by the square of impression A within 30 sec. of loading.

$$H = \frac{P_{max}}{A} \tag{1}$$

The impression on PTFE surface is very difficult to be optically distinguished and for its measurements necessarily to create a special coating on the surface, to observe the impression in the reflection light. The standard ISO 2039/1-87 assumes also possibility to determine the square of impression projection using impression depth α with the help of displacement sensor. In this case hardness is calculated by follows:

$$H = \frac{P_{max}}{\pi D \alpha_{max}}, \tag{2}$$

where D is the diameter of the indenter tip, α_{max} is maximum of the indentation depth.
Disadvantage of equation (2) consists in dependence of measurement result on the indentation depth, because P_{max} and α_{max} are changed in non-proportional manner. In fig 1 the behaviour of changing of the static hardness H_s against P_{max} for the samples from PTFE is presented. The measurements carried out on Vickers hardness meter using the

indenter with tip diameter equal to 5 mm. at the loading ranged from 50 to 400 N. Simultaneously the registration of the indenter displacements was conducted. As can see in fig.1 at the same load we received different values of hardnesses.

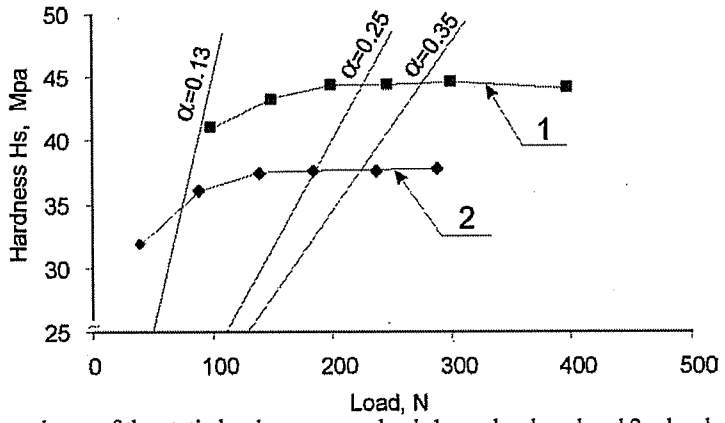

Fig. 1. Dependence of the static hardness versus load. 1- nonhardened and 2 – hardened PTFE.

For the removal of this ambiguity it was adopted to determine hardness at given constant value of the indentation depth equal to 0,25mm. According to this proposal the loadings should be equal to 49,1; 132; 358; 961N. Indentation depth should be in a range from 0,13 to 0,35 mm and the loading corresponding to the depth of 0,25 have to be determined by means of recalculation [1]. Straight lines in fig.1 corresponding indentation depths α=0,13, 0,25 and 0,35 mm are shown.

The process dynamic indentation is different from static one. During dynamic indentation additional resistance to indenter intrusion is occurred, which depends on impact velocity and chemical composition of polymeric material. Hard polymeric materials are deformed in plasticity manner when contact pressure is more than its yield stress. As it was experimental established, residual impression can be seen on tested surface of PTFE materials in the research temperature range from –10 up to +80 C°. In this case elastic-plastic properties are more pronounced than viscous-elastic ones. The last is confirmed by a small change of impression diameter measured immediately at the impact and after some minutes. However at temperature more than 80 C° change in impression diameter is increased up to 7%.

In fig. 2 dependence of the dynamic hardness, calculating from formula (2) versus different loading values is shown Variation of loading is carried out by the change of initial impact velocity V .The testing was made with the help installation IMPULSE - 1R which was designed in the Institute of Applied Physic of the National Academy of Science of Belarus and NPO Energomash, Khimki (Russia). As can see character of smooth increasing of dynamic and static hardness against loading is the same in considered range of contact forces up to 60 N, but values of dynamic hardness always higher than static one. In order to explain this excess it can use the model of polymeric materials deforming at different velocities [2]. In accordance with the model it can write expression for pressure, which equal yield stress, as follows

$$\sigma_d = A + B\ln[a_T(\bar{\varepsilon}'_d/\bar{\varepsilon}'_{cr})], \qquad (3)$$

where A, B and a_T are coefficients which depend on chemical composition and temperature, $\bar{\varepsilon}'_{cr}$ and $\bar{\varepsilon}'_d$ are mean strain rates at dynamic and static intrusion on given indentation depth.

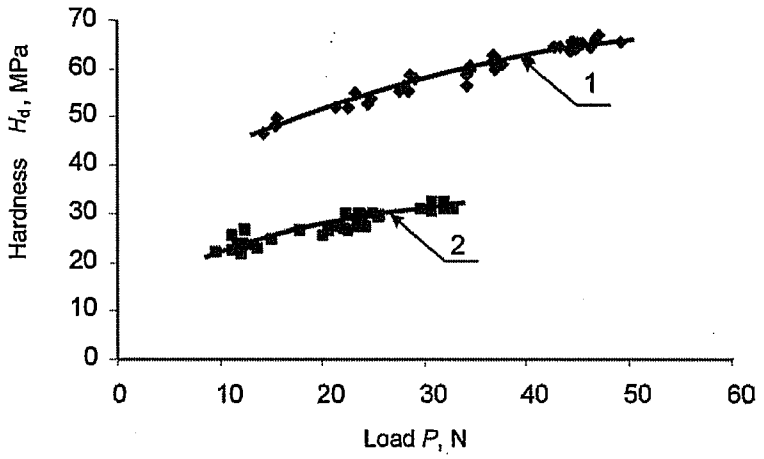

Fig. 2. Dependence of the dynamic hardness versus load. 1- nonhardened and 2 – hardened PTFE.

After some transforms we obtain

$$\sigma_d = \sigma_{ст} + B\ln(\dot{\bar{\varepsilon}}_d / \dot{\bar{\varepsilon}}_{ст}), \quad (4)$$

where $\sigma_{ст} = A + B\ln(a_T)$ is pressure at static loading. As can see in the case, when $\dot{\bar{\varepsilon}}_{ст} = \dot{\bar{\varepsilon}}_d$ static and dynamic pressure will be equal $\sigma_d = \sigma_{ст}$.

Taking into account that hardness is pressure, measuring at certain strain, equation (4) can be wrote as follows

$$H_d = H_{ст} + B\ln(\dot{\bar{\varepsilon}}_d / \dot{\bar{\varepsilon}}_{ст}) \quad (5)$$

Since hardness value is function strain, it is necessary to determine strain value corresponding strain applied in above mention the static test at intrusion $\alpha = 0{,}25$ mm. Evaluating strain value as

$$\varepsilon = 0{,}2\frac{d}{D}, \quad (6)$$

where $d = 2\sqrt{D\alpha}$ is diameter of impression projection, we determine $\varepsilon = 0{,}087$.

With the help of equation (5) we can calculate intrusion depth at given strain and diameter of the indenter tip

$$\alpha = 6{,}25D\varepsilon^2 \quad (7)$$

In installation IMPULSE - 1R diameter D of the indenter tip is 1mm.and formula (6) show that α should be no less than 50 μm. In fig 3 typical diagrams: contact force versus displacement, which were obtained during impact test of PTFE products are presented.

From the fig. 3 it can see follows the characteristic feature of PTFE. The dependence of the contact force versus penetration on the active stage of impact is invariable on initial velocities of the impact in the range from 0,5 to 1,5 m/s. This fact confirms that the properties of PTFE are very closely to the properties of elastic-plastic materials. As can be seen, the dependences of the contact force vs penetration are similar and by only the values of maximum forces and penetrations are characterized. It means that at the given strain rates the second term in the equation (5) will be in insignificant degree depend on the strain rate at the dynamic testing.

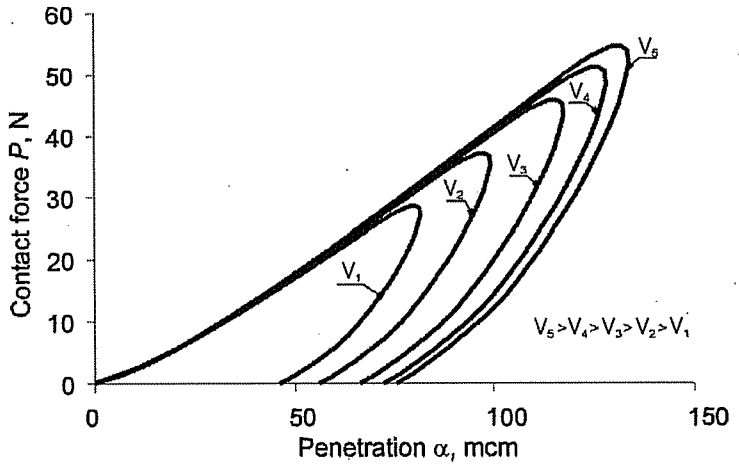

Fig. 3. Typical dependencies contact force-penetration at the dynamic testing of PTFE with different initial velocity: 1 – 0,5; 2 – 1,0; 3 – 1,2; 4 –1,35; 5 – 1,5 m/s.

Actually, the estimation of the values of the strain rate at the testing with the help of static and dynamic method showed that the value of logarithm in (5) changes in the limits from 7,5 to 10. At the static testing according to ISO 2039/1 load is applied during 1-2 seconds, after that the load is sustained by the 30 second. During this process the diameter of the impression increases due to creep, but the finishing value of the impression on the hardened PTFE is greater than initial impression but not more than 4 %. Taking into account that the deformation, which necessary to attain at the tests, is 0,087, the average rate of the static strain will be $\frac{\varepsilon}{t} = \frac{0{,}087}{1{,}5} \approx 0{,}06$ s^{-1}. The average strain rate at the dynamic testing at the temperature in the range of -10 to + 80 ^{0}C will be varied in the limits of 100-600 s^{-1}.

In the Figure 4a the change of the values of logarithm $\ln(\bar{\varepsilon}_d'/\bar{\varepsilon}_s')$ versus initial velocity of the indenter V_0 for one of the PTFE samples is shown.

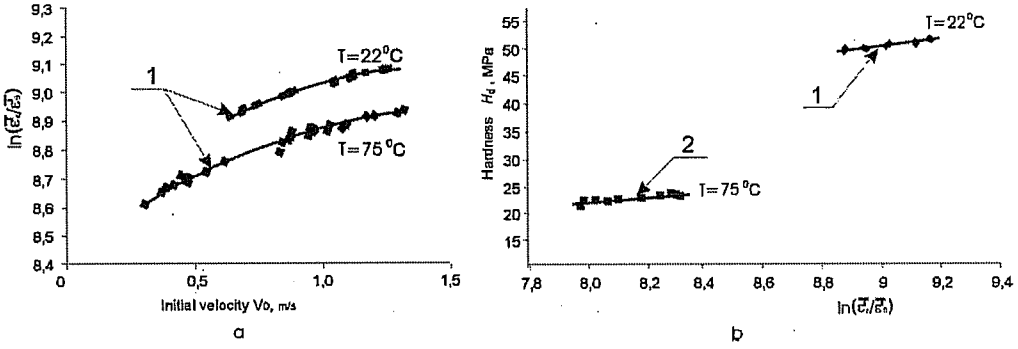

Fig. 4. a) Dependence of $\ln(\bar{\varepsilon}_d'/\bar{\varepsilon}_s')$ in the equation (5) versus initial velocity of the indenter; b) dependence of the dynamic hardness against $\ln(\bar{\varepsilon}_d'/\bar{\varepsilon}_s')$. 1- nonhardened and 2 – hardened samples.

The change of $\ln(\bar{\varepsilon}_d'/\bar{\varepsilon}_s')$ is small, although slightly depends on the temperature, strain rate, and degree of crystallinity (i.e. structure and properties of PTFE). In the figure 4b the change of the dynamic hardness for the samples of PTFE with different degree of crystallinity at the different temperatures is shown. As it follows from the dependences,

reflected in figure 4a, the difference in the value of logarithm $\ln(\bar{\varepsilon}_d'/\bar{\varepsilon}_s')$ is characteristic only for PTFE in the whole investigated temperature and strain rate ranges, and furthermore it depends on the degree of crystallinity (i.e. structure and of the properties of PTFE). Consequently, the real change in the hardness, caused by the change in the strain rate (in the investigated range of initial velocities from 0,5 to 1,5 m/s) insignificantly and does not exceed 5 %. It means that the value of $\ln(\bar{\varepsilon}_d'/\bar{\varepsilon}_s')$ can be accepted to be constant at a certain temperature.

The change of the hardness at different temperatures will be determined by the structural and temperature-sensitive coefficient **B.** In this case equation (5) will be exact not only for the average values of the strain rate, but also for its instantaneous values $\varepsilon'(t)$ at the given moment of time. This gives an opportunity to determine the static hardness using the dynamic measurements.

In the Figure 5 the change of the hardness in the process of the indenter intrusion at the dynamic and static tests is shown. As can be seen from the figure the value of dynamic hardness (stress) differs and higher the static stress on the certain practically constant value. This is the result of the fact that the change of the logarithm in the given range of strain rate differs insignificantly.

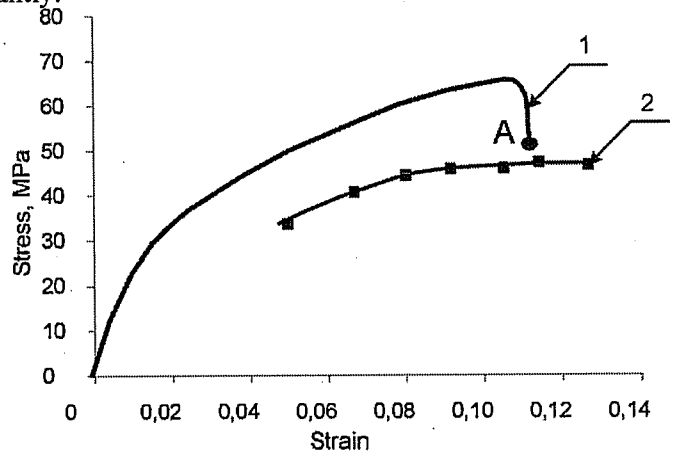

Fig. 5. Dependence of stress versus strain at the dynamic (1) and static (2) testing.

Furthermore, at the sharp reduction of the strain rate at the end of the impact until zero, static and dynamic hardness practically coincide (point A in the figure 5). The small exceeding of dynamic hardness in this case can be explained by the influence of the viscous properties of PTFE, which were not taken into consideration. In practice, as a rule, accepted to evaluate the properties of material by the static hardness value. Taking into account that the strain rate at the dynamic measurements practically does not changes, the value of logarithm $\ln(\bar{\varepsilon}_d'/\bar{\varepsilon}_s')$ can be considered as the constant, equal to 8,6. After division of equation for H_d by H_s we will obtain that $\frac{H_d}{H_s} = K_d$, where $K_d = 1 + B\ln(\bar{\varepsilon}_d'/\bar{\varepsilon}_{cm}')/H_s$ is dynamic coefficient for the given temperature. The existence of this coefficient speaks about the possibility of the determination of the static hardness from the results of its determination at the dynamic testing. In the figure 6 the experimental dependence, obtained at the testing of PTFE with different degree of crystallinity in the range of temperatures from -10 to +80 ^{0}C is shown.

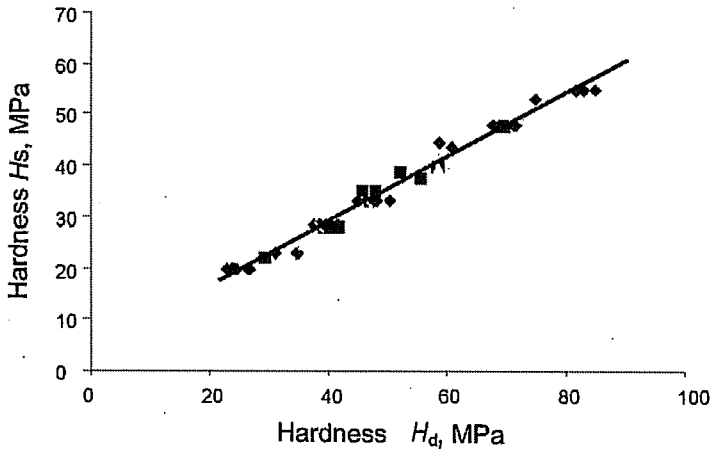

Fig. 6. Relation between the static and dynamic hardness for PTFE with different crystallinity.

Correlation coefficient of this dependence is 0,982 and presented dependence can be described by the equation (8).

$$H_s = 0{,}624 H_d + 4{,}511 \text{ (MPa)} \quad (8)$$

As practice showed, the error in the determination of static hardness from the results of dynamic measurements does not exceed 6%. In this connection it is possible to assert that at the condition $\varepsilon_s = \varepsilon_d$ the static hardness can be found with simple conversion with the help of equation (8).

References

[1] ISO 2039/1-2001 Plastics. Determination of hardness. Ball indentation method
[2] *Racke H.H., Fett T.* / Materialprufung, 1968. Bd. 10, N 7, P.226–230.

Exhibit 50

PROCEEDINGS

OF THE

ROYAL SOCIETY OF LONDON

SERIES A. MATHEMATICAL AND PHYSICAL SCIENCES

VOL. 192

LONDON
Printed and published for the Royal Society
By the Cambridge University Press
Bentley House, N.W.1

18 March 1948

A simple theory of static and dynamic hardness

By D. Tabor, *Research Group on the Physics and Chemistry of Rubbing Solids, Department of Physical Chemistry, University of Cambridge*

(*Communicated by Sir Geoffrey Taylor, F.R.S.—Received* 17 *May* 1947)

When a hard spherical indenter is pressed into the surface of a softer metal, plastic flow of the metal specimen occurs and an indentation is formed. When the indenter is removed it is found that the permanent indentation is spherical in shape, but that its radius of curvature is greater than that of the indenter. It is generally held that this 'shallowing' effect is due to the release of elastic stresses in the material around the indentation. It is clear that if the recovery is truly elastic it should be reversible and that a second application and removal of the indenter under the original load should not change the size or shape of the indentation. Experiments show that this is the case. This means that when the original load is reapplied, the deformation of the indenter and the recovered indentation is elastic and should conform with Hertz's equations for the elastic deformation of spherical surfaces. Measurements show that there is, in fact, close agreement between the observed deformation and that calculated from Hertz's equations.

These results have been applied to the case of indentations formed in a metal surface by an impacting indenter. The energy involved in the elastic recovery of the impacting surfaces is found to account for the energy of rebound of the indenter. This analysis explains a number of empirical relations observed in dynamic hardness measurements, and, in particular, reproduces the calibration characteristics of the rebound scleroscope. The results also show that for very soft metals the dynamic hardness is very much higher than the static hardness, and it is suggested that in rapid deformation of soft metals, forces of a quasi-viscous nature are involved.

In the third part of the paper a simple theory of hardness is given, based on the theoretical work of Hencky and Ishlinsky. It is shown experimentally that for a material incapable of appreciable work-hardening, the mean pressure P_m required to produce plastic yielding is related to the elastic limit Y of the material by a relation $P_m = cY$, where c is a constant having a value between 2·6 and 3. An empirical method is described which takes into account the work-hardening produced in metals by the indentation process itself. This results in a general relation between hardness measurements and the stress-strain characteristic of the metal, and there is close agreement between the theory and the observed results. In addition, the theory explains the empirical laws of Meyer.

1. Static hardness measurements

The hardness of a metal is often defined as its resistance to indentation (O'Neill 1934). In the Brinell hardness test (Brinell 1900; Meyer 1908), a hard steel ball is pressed under a fixed normal load on to the smooth surface of the metal to be tested. When equilibrium has been reached, the load and indenter are removed, and the diameter of the permanent impression measured. The hardness is then expressed as the ratio of the load to the curved area of the indentation (Brinell hardness) or as the ratio of the load to the projected area of the indentation (Meyer hardness). In both cases, the hardness has the dimensions of pressure.

The relation between load and size of indentation may be expressed by a number of empirical relations. The first of these, known as Meyer's law, states that if F is the load applied and d the diameter of the impression left when the indenter is removed

$$F = kd^n, \tag{1}$$

where k and n are constants for the material when the diameter of the ball is fixed. The value of n is generally greater than 2 and usually lies between 2 and 2·5. For completely unworked materials, n has a value near 2·5, whilst for fully worked materials it is close to 2.

When balls of different diameters are used, the values of these constants change. For balls of diameters $D_1, D_2, D_3, \ldots$ giving impressions of diameters $d_1, d_2, d_3, \ldots$, a series of relations is obtained of the type

$$F = k_1 d_1^{n_1} = k_2 d_2^{n_2} = k_3 d_3^{n_3}. \tag{2}$$

In a very extensive series of investigations Meyer (1908) found experimentally that the index n was almost independent of D but that k decreased with increasing D in such a way that

$$A = k_1 D_1^{n-2} = k_2 D_2^{n-2} = k_3 D_3^{n-2} = \ldots, \tag{3}$$

where A is a constant.

When conical or pyramidal indenters are used as in the Ludwik and Vickers hardness tests respectively a simpler relationship is observed. Over a wide range of experimental conditions it is found that

$$F = kd^{2\cdot0} \tag{4}$$

for an indenter of fixed angle. The power of d is fixed, but k depends upon the angle of the cone or pyramid used.

It has long been known that the permanent indentation left in a metal surface deformed by a hard steel ball has a larger radius of curvature than that of the indenting sphere. Some very careful measurements by Foss & Brumfield (1922) have shown that the indentation is symmetrical and of spherical form, but that its radius of curvature may, for hard metals, be as much as three times as large as that of the indenting sphere. This effect has generally been ascribed to the release of elastic stresses in the metal specimen, but little work of an analytical nature has been carried out to relate this to the elastic properties of the metal and the ball.

It is at once evident that if the recovery observed is an elastic one, it should be essentially reversible. That is to say, if the indenter is replaced in the recovered indentation and the original load applied, the surfaces should deform elastically, and on removing the load, the diameter and curvature of the recovered indentation should be unchanged.

Experiments were carried out to test this. A series of impressions were made with hard steel balls of various diameters on various metal surfaces, using loads ranging from 250 to 3000 kg. The diameters d of the impressions formed were measured after 1, 2, 3 and 5 cyclic applications of the load. The radius of curvature r_2 of the recovered indentation was also measured, using (a) a delicate profilometer, (b) a metallographic section across the diameter of the indentation. The values of d were reproducible to less than 1 %. The radii of curvature as determined by the profilometer method were reproducible to about 4 %. A few of these values were compared with those obtained from direct photomicrographs of the sections across the diameter of the

indentation; the agreement was of the order of 1 to 2 %. For example, with a single application of load of 500 kg. on mild steel (10 mm. ball) the radius of curvature of the indentation by the profilometer method (mean of three determinations) was 0·595 cm. and by the direct contour method 0·605 cm. These values are typical. The results are given in table 1.

TABLE 1

metal	radius of ball r_1 (cm.)	load (kg.)		dimensions of indentations (cm.) number of applications of load 1	2	3	5
brass	0·952	500	d	0·27	0·270	0·270	0·270
			r_2	1·21	1·21	1·19	1·20
aluminium alloy	0·952	500	d	0·26	0·260	0·263	—
			r_2	1·15	1·16	1·16	—
mild steel	0·5	500	d	0·183	0·185	0·186	0·192
			r_2	0·595	0·585	0·55	—
hardened steel	0·5	1000	d	0·202	0·200	0·203	0·206
			r_2	0·677	0·677	0·68	0·652
	0·952	3000	d	0·330	0·330	0·338	0·338
			r_2	1·39	1·37	1·31	1·37
	1·59	3000	d	0·370	0·366	0·366	0·365
			r_2	5·60	5·54	5·68	5·41

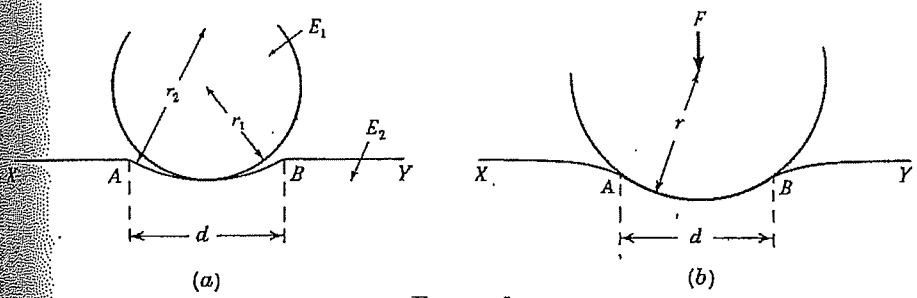

FIGURE 1

It is seen that the indentation remains essentially unaltered in diameter and curvature after the second and third applications of the original load. This shows that the deformation occurring at the final stage of the original deformation is reversible and is therefore essentially elastic.

Since the 'recovery' of the indentation is truly elastic, it is possible to apply the classical laws of elasticity to this portion of the deformation process. The condition of the surface of the metal after the indentation has been formed is idealized, and it is assumed that it consists of a plane surface $XABY$ containing a depression of spherical form of radius of curvature r_2 and of diameter $d = 2a$ (figure 1 a).

When a hard steel sphere (radius of curvature r_1) is placed in the indentation, and a normal force of F dynes is applied, both surfaces are elastically deformed to a common radius of curvature r where $r_2 > r > r_1$ and the deformed surfaces finally

touch over the boundaries of the indentation (figure 1*b*). It is assumed that there is very little change in the diameter d during this deformation, an assumption which is generally accepted as being valid to within a few per cent. Then, according to Hertz's classical equations (Hertz 1896) describing the elastic deformation of spherical surfaces, the relationship between d, r_1 and r_2 is given by

$$d = 2a = 2{\cdot}22\left[\frac{F}{2}\frac{r_1 r_2}{r_2 - r_1}\left(\frac{1}{E_1}+\frac{1}{E_2}\right)\right]^{\frac{1}{3}}, \tag{5}$$

where E_1, E_2 are Young's moduli for the indenter and the metal, and where a value of 0·3 for Poisson's ratio has been assumed.

In a discussion of the derivation of this equation, Prescott (1927) has indicated that even if the surface $XABY$ is not a plane, the same equation will result. If, for example, the surface rises at the regions A and B as in figure 2*a* or falls as in figure 2*b*, the above equation is still valid, provided the projections or depressions at A and B are not too marked.

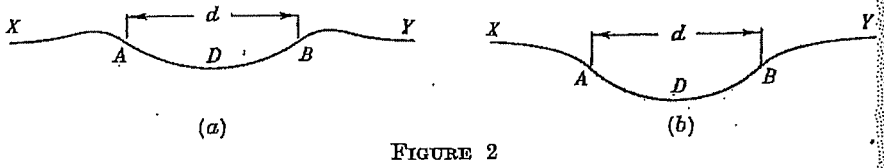

FIGURE 2

This equation is applied to the previous measurements of r_1, r_2, F and d. The value of d obtained from equation (5) is compared with the observed value of the diameter of the recovered impression. The results are given in table 2. It is seen that the agreement between the last two columns is reasonably good, particularly as the accuracy in determining r_2 is not better than about 4 %.

TABLE 2

material	assumed value of E_1 (dynes/cm.^{2})	load (kg.)	observed values (cm.) r_1	r_2	d	calculated d (cm.)
brass	10×10^{11}	250	0·5	0·64	0·160	0·17
		500	0·952	1·21	0·27	0·26
aluminium alloy	7×10^{11}	250	0·5	0·66	0·178	0·18
		500	0·952	1·15	0·26	0·30
mild steel	20×10^{11}	500	0·5	0·605	0·183	0·20
hardened steel	20×10^{11}	1000	0·5	0·677	0·202	0·22
		3000	0·952	1·39	0·330	0·36
		3000	1·59	2·80	0·370	0·39

As a matter of interest, use is made of the observations of earlier workers.

(1) Profiles given by Batson (1918) for a ball of diameter 10 mm. and a load of 3000 kg. on three types of steel. It is assumed that $E_2 = 20\times10^{11}$ dynes/cm.^{2} for

all the steels. The results are given in table 3. It is seen that the agreement between the observed and calculated values of d is reasonably good.

TABLE 3

material	observed values r_1 (cm.)	r_2 (cm.)	d (cm.)	calculated d (cm.)
Ni-Cr steel	0·5	0·627	0·324	0·34
manganese steel	0·5	0·569	0·407	0·41
rail steel	0·5	0·537	0·445	0·49

(2) Profiles given by Foss & Brumfield (1922) for a ball of 10 mm. diameter on various brasses. The results are tabulated in table 4. It is seen that the agreement for the smaller loads (500 kg.) is good, whilst the agreement for the higher loads (3000 kg.) is poor. This is probably because for soft metals the values of r_2 are very little different from r_1 for high loads, so that the errors introduced in calculating $r_1 r_2/(r_2 - r_1)$ may be very large. In table 5 results are taken where r is greater than 0·55 cm.

TABLE 4

	assumed value of E_2 (dynes/sq.cm.)	load (kg.)	observed values r_1 (cm.)	r_2 (cm.)	d (cm.)	calculated d (cm.)
soft brass 1	9×10^{11}	3000	0·5	0·518	0·555	0·7
soft brass 2	9×10^{11}	500	0·5	0·521	0·330	0·38
hard bronze 3	$7·5 \times 10^{11}$	3000	0·5	0·527	0·497	0·66
soft bronze 4	$7·5 \times 10^{11}$	500	0·5	0·557	0·276	0·28
hard bronze 5	$7·5 \times 10^{11}$	3000	0·5	0·531	0·499	0·63
soft bronze 6	$7·5 \times 10^{11}$	500	0·5	0·566	0·302	0·28

(3) Profiles given by Foss & Brumfield (1922) for a ball of 10 mm. diameter and a load of 3000 kg. on various steels. It is assumed that $E_2 = 20 \times 10^{11}$ dynes/cm.^{2} for all the steels. The results are given in table 5, and it is seen that the agreement between d (calculated) and d (observed) is close.

TABLE 5

metal	observed values r_1 (cm.)	r_2 (cm.)	d (cm.)	calculated d (cm.)
0·5C-A	0·5	0·56	0·440	0·43
0·5C-O	0·5	0·593	0·342	0·37
0·5C-T	0·5	0·701	0·345	0·31
0·5C-W	0·5	1·03	0·26	0·25
0·5C-T	0·5	0·652	0·30	0·32
0·9C-T	0·5	0·814	0·31	0·28
0·9C-O	0·5	0·644	0·301	0·33
0·9C-W	0·5	1·372	0·240	0·23
MKD 455	0·5	0·568	0·349	0·36

These results show that in general the agreement between the observed and calculated values of d is reasonably good, particularly when r_2 is not too close to r_1, i.e. when the elastic 'recovery' is marked. It is, of course, true that as the calculation of d involves a cube root, the values of F, r_1, r_2, E_1 and E_2 are not very critical. Nevertheless, the agreement is consistent for a great diversity of materials and experimental conditions.

Discussion

The experiments show that when an indentation is formed in a metal surface by a hard spherical indenter, the last stage of the indentation process is reversible and may be expressed in terms of the elastic constants of the materials and the sphere. This is shown by the fact that after several cyclic applications of the original load the recovered indentation remains essentially unaltered in diameter and in radius of curvature. Further, the extent of the elastic 'recovery' of the indentation may be calculated on the basis of Hertz's equations, and the results show that on the whole there is good agreement between the observed and calculated values for a wide range of materials and experimental conditions.

The following mechanism for the processes involved in the Brinell hardness test may, therefore, be put forward. When the ball presses on to the surface, the metal is first deformed elastically. The stresses, however, soon exceed the elastic limit of the metal and plastic flow occurs. As the metal is displaced, work-hardening occurs and the elastic limit of the material increases (see, for example, the description in Carpenter & Robertson (1936)). This process continues until the stresses are now distributed over an impression of such dimensions that the stresses are within the elastic limit of the deformed material. At the end of the process, therefore, plastic flow has ended and the whole of the load is borne by elastic stresses in the material. If, for example, the load is removed, there is elastic 'recovery', and if the same load is reapplied, the surfaces deform elastically until they just fit over the diameter of the original impression. The elastic stresses now reach the limits that the deformed material around the impression can stand. If the load is removed or reduced, there is, as we have seen, a release of elastic stresses. If it is further increased, the stresses exceed the elastic limit and further flow of the material occurs. There is a further increase in work hardening and the process continues until the stresses are distributed over a larger impression, and so fall again within the increased elastic limit.

2. Dynamic hardness measurements

If a hard steel or diamond indenter is dropped on to a metal surface, it rebounds to a certain height and leaves an indentation in the surface. Martel (1895) showed that over a wide range of experimental conditions, the volume of the indentation so formed is directly proportional to the energy of the indenter. Vincent (1900) and other workers have confirmed this experimental observation. This result may be interpreted as implying that the metal offers a constant pressure of resistance to the indenter equal numerically to the ratio (energy of indenter)/(volume of indentation).

This ratio has the dimensions of pressure, and is referred to as the dynamic hardness number. Later workers have discussed the validity of this relation in some detail, and in particular it has been suggested that the energy of rebound should be taken into account in calculating the dynamic hardness.

A different approach is that adopted in Shore's scleroscope, where the height of rebound is used as a measure of hardness. It is found that if the height of fall is constant, the height of rebound is roughly proportional to the static hardness of the material concerned (Shore 1918).

In what follows the processes involved in impact experiments will be analyzed, a simple theory which explains a number of empirical relations observed in dynamic hardness measurements will be developed.

The process of impact may be divided into three main parts. (i) When the indenter first strikes the metal surface, elastic deformation takes place until the mean pressure developed is sufficient to cause plastic flow of the metal. (ii) Plastic deformation of the metal now occurs accompanied by a building up of further elastic stresses in both the indenter and the metal. This process continues until the indenter is brought to rest. (iii) There is now a release of elastic stresses in the indenter and the material surrounding the indentation, as a result of which rebound occurs.

In a detailed investigation of the impact of spheres of similar metals, Andrews (1930), who was mainly concerned with the period of the collision, calculated the time involved in each of these portions of the impact. The analysis applied to the last two parts of the process was, however, of an admittedly approximate nature. In the following analysis, where one is concerned essentially with the forces involved and not the time of collision, a different procedure which considerably simplies the problem will be adopted.

It is assumed that there is a dynamic yield pressure P which to a first approximation is constant and which is not necessarily the same as the static pressure necessary to cause plastic flow. This assumption implies that whenever the pressure during impact reaches the value P, plastic flow occurs, and so long as plastic flow continues the pressure remains constant at this value. Now consider the indentation after impact has occurred. If the volume of the remaining permanent indentation is V_r, the work done as plastic energy in producing this indentation is by definition of P given by

$$W_3 = PV_r. \tag{6}$$

Clearly the energy W_3 is the difference between the energy of impact W_1 and the energy of rebound W_2. All that remains therefore is to calculate W_2 and the volume V_r.

Suppose the indenter has a mass m and a spherical tip of radius of curvature r_1 and that it falls from a height h_1 on to a flat metal surface. After the collision the indenter rebounds to a height h_2 and leaves a permanent indentation in the metal surface of diameter $d = 2a$. It is assumed that the mechanism involved in the dynamic indentation is essentially the same as that which occurs under static conditions. That is to say, when the plastic deformation has been completed, there is a residual elastic deformation which is reversible. It is assumed that the energy

involved in the release of these elastic stresses is equal to the energy of rebound of the indenter. Finally, it is assumed that Young's moduli for the indenter and the metal are essentially the same as for static conditions.

Again, consider the indentation after the impact has occurred. Since there has been a release of elastic stresses in the indentation, its radius of curvature will not be r_1 but will be somewhat greater, say r_2. If a suitable load F were applied to the indenter for a very short interval, it would deform the indentation (and itself) elastically, and just touch over the diameter d, where again

$$d = 2a = 2{\cdot}22\left[\frac{F}{2}\frac{r_1 r_2}{r_2 - r_1}\left(\frac{1}{E_1}+\frac{1}{E_2}\right)\right]^{\frac{1}{3}}. \tag{5a}$$

The elastic energy involved in this process is estimated by calculating the external work performed in pressing the indenter into the indentation. As the indenter sinks into the indentation the force increases from zero and reaches the final value F given by equation (5a) as the full contact across the diameter $d = 2a$ is completed. At any intermediate instant when the region of contact has a diameter 2α (where $\alpha < a$) the force f on the indenter, given by equation (5a), is

$$f = F\frac{\alpha_3}{a^3}. \tag{5b}$$

At this stage, as a result of the elastic deformation of both contacting surfaces, the centre of the indenter has descended a distance z (Prescott 1927) given by

$$z = \frac{3f}{4\alpha}\left[\frac{1-\sigma_1^2}{E_1}+\frac{1-\sigma_2^2}{E_2}\right], \tag{7}$$

where σ_1 and σ_2 are Poisson's ratio for the indenter and the anvil respectively. Then the integral of $f\,dz$ over the range $\alpha = 0$ to $\alpha = a$ is the total elastic energy stored in the surfaces. A simple integration shows that this energy, which we equate to the energy of rebound, is

$$W_2 = mgh_2 = \frac{0{\cdot}27F^2}{a}\left[\frac{1}{E_1}+\frac{1}{E_2}\right], \tag{8}$$

where a value of 0·3 is again assumed for Poisson's ratio.

The volume V_r of the permanent indentation left in the surface may be written to a first approximation as $V_r = \pi a^4/4r_2$.

Hence
$$W_3 = W_1 - W_2 = PV_r = P\frac{\pi a^4}{4r_2}. \tag{6a}$$

We now express r_2 in terms of r_1 and F from equation (5a),

$$\frac{1}{r_2} = \frac{1}{r_1} - 0{\cdot}68\frac{F}{a^3}\left[\frac{1}{E_1}+\frac{1}{E_2}\right]. \tag{5c}$$

Hence
$$W_3 = P\frac{\pi a^4}{4r_1} - 0{\cdot}17\frac{F^2}{a}\left[\frac{1}{E_1}+\frac{1}{E_2}\right], \tag{9}$$

since the force F at end of indentation is equal to $P\pi a^2$. The first term of equation (9) is simply PV_a, where V_a is the *apparent* volume of the indentation which would be obtained if the indentation was considered to have the same radius of curvature as the indenter. The second term, by comparison with equation (8), is seen to be equal to $\frac{5}{8}W_2$. Hence

$$W_3 = PV_a - \tfrac{5}{8}W_2. \tag{10}$$

Thus

$$P = \frac{mg(h_1 - \frac{3}{8}h_2)}{V_a}. \tag{11}$$

The validity of this analysis depends on the assumption that the internal forces occurring in the actual impact are essentially the same as those involved in the analytical model just described. In particular, it is assumed that the elastic waves set up in the indenter and the metal specimen absorb a negligible amount of energy. It is also assumed that the temperature rise of the material around the indentation during the impact is small and has a negligible effect on the strength properties of the metal.

It is at once apparent that if the rebound is not very large (so that h_2 is small) the results will not be very different from the equation given by Martel, $P = mgh_1/V_a$, nor from the equation suggested by later workers, $P = mg(h_1 - h_2)/V_a$.

Effect of variation in the value of P

In the above derivation it has been assumed that P is a constant throughout the process of impact. There are, however, two reasons why P may be expected to vary during the collision. The first is a dynamic effect associated with the kinetic displacement of the metal during impact. This will tend to increase P at the initial stages of the deformation when the velocity of displacement is a maximum (see later). It is difficult, however, to express this effect quantitatively. The second reason is that work hardening of the deformed material will occur during the formation of the indentation. As a result, P will tend to increase during impact in a manner similar to that observed in static hardness measurements, as described in equation (1). Some estimate of the order of this effect may be made by assuming that, on analogy with the static indentations, we can write

$$P = kd^{n-2}, \tag{1a}$$

where n lies between 2 and 2·5. Then the work W_3 expended in displacing plastically a volume V_r becomes

$$W_3 = \frac{4}{n+2}PV_r, \tag{6a}$$

where P is now the mean pressure at the *end* of the deforming process. This is also the pressure involved in the calculation of the rebound. Substituting this value of W_3 in the appropriate equations, we obtain

$$P = \frac{n+2}{4}\frac{mg\left(h_1 - \dfrac{2n-1}{2(n+2)}h_2\right)}{V_a}. \tag{11a}$$

The last term in the bracket varies from $\frac{3}{8}h_2$ to $\frac{4}{9}h_2$ as n varies from 2 to 2·5, so that this term tends to give lower values for P. On the other hand, the term in front of the main bracket increases from 1 to 1·12 as n increases from 2 to 2·5. The total effect is to give values of P which are somewhat greater than those given in equation (11). The difference, however, will never be more than about 10 %.

The validity of equations (8) *and* (11)

Remembering that at the end of the indentation process, $F = \pi a^2 P$, we rewrite equation (8) as

$$h_2 = \frac{2{\cdot}7a^3P^2}{mg}\left[\frac{1}{E_1}+\frac{1}{E_2}\right]. \qquad (8a)$$

Since the apparent volume of the indentation V_a is proportional to a^4, this means that h_2 is proportional to $V_a^{\frac{3}{4}}$ for any fixed material. Plotting h_2 against V_a on logarithmic ordinates, straight lines should be obtained with a slope of $\frac{3}{4}$, if P is constant. Some results taken from Edwards & Austin's paper (1923) are plotted in figure 3, and it is seen that this is approximately true. If P is not constant but varies in the manner given by equation (1a) it is found that the logarithmic graph of h_2 against V_a is still a straight line, but the slope has a value of $\frac{1}{4}(3+2n-4)$, i.e. it varies from $\frac{3}{4}$ to 1 as n varies from 2 to 2·5. It is seen from figure 3 that in fact the points for each material lie on a straight line, and that the slope lies between 0·7 and 0·85.

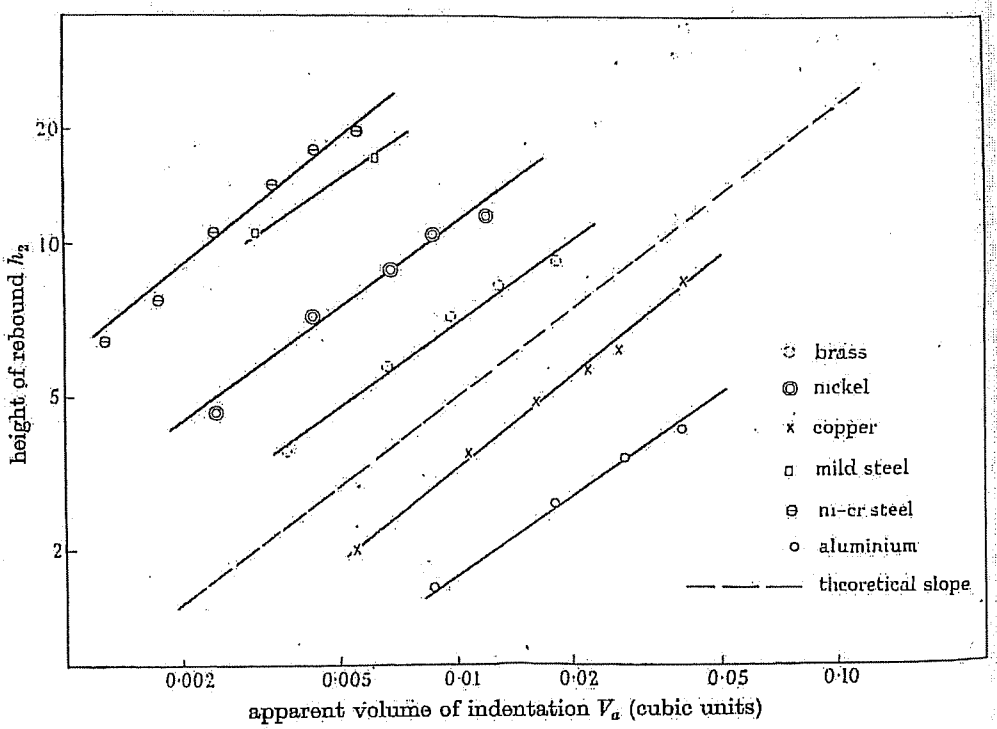

FIGURE 3

Again, for indentations of a fixed diameter, h_2 should be proportional to $P^2[1/E_1+1/E_2]$. If, therefore, h_2 is plotted against $P\sqrt{(1/E_1+1/E_2)}$ on logarithmic ordinates, a straight line of slope $\frac{1}{2}$ should be obtained. Results taken from the same paper are plotted in figure 4, the values of P being calculated according to equation (11). There is again good agreement, the slope of the straight line being 0·51. In this case, any dependence of P on the size of the indentation does not appreciably affect the relation.

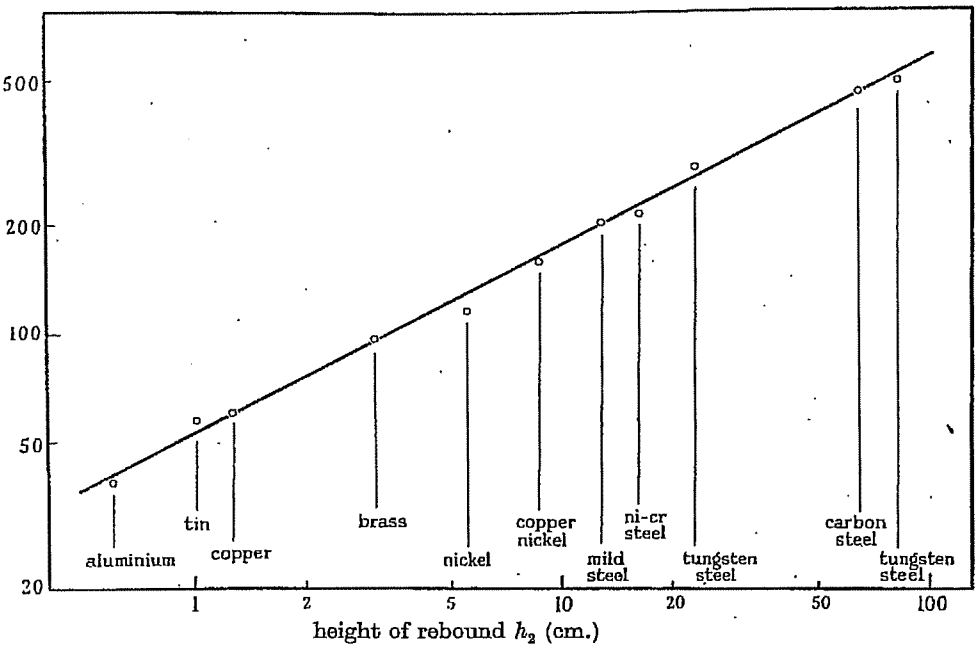

FIGURE 4

Finally, a may be eliminated between equations (8a) and (11). The resulting relation between h_1, h_2 and P is given by

$$P^5 = \frac{h_2^4}{(h_1-\frac{3}{8}h_2)^3}\frac{mg}{109r_1^3[1/E_1+1/E_2]^4}. \qquad (12)$$

(A similar relation is obtained if equation (11a) is used instead of equation (11).)

Since the bracket involving Young's moduli does not vary greatly for most metals, this factor may be treated as a constant and P may be plotted as a function of h_2 for a given height of fall h_1. The theoretical curve is shown in figure 5.

If allowance is made for the fact that softer metals usually have a smaller Young's modulus, the curve is modified in a manner similar to that shown in the dotted curve. These curves reproduce in fact the main characteristics observed in the practical calibration of rebound sclerescopes. It is also evident that over a wide range of experimental conditions the height of rebound, for a fixed height of fall, is almost directly proportional to the dynamic yield pressure.

The condition for elastic collisions

It is interesting to consider what happens when the rebound is equal to the height of fall. In this case, the processes of impact and rebound become entirely elastic, and there is no plastic deformation of the anvil (see Taylor 1946). If we go back to the original equations and calculate the final average pressure P_e developed between the indenter and the anvil in a purely elastic collision, we obtain a relation

$$P_e^5 = \frac{1}{26{\cdot}6\pi_1^3}\frac{mgh_1}{(1/E_1+1/E_2)^4}, \qquad (12a)$$

again assuming a value of 0·3 for Poisson's ratio. This is exactly the same as the value for P obtained from equation (12) when h_2 is put equal to h_1. Two conclusions

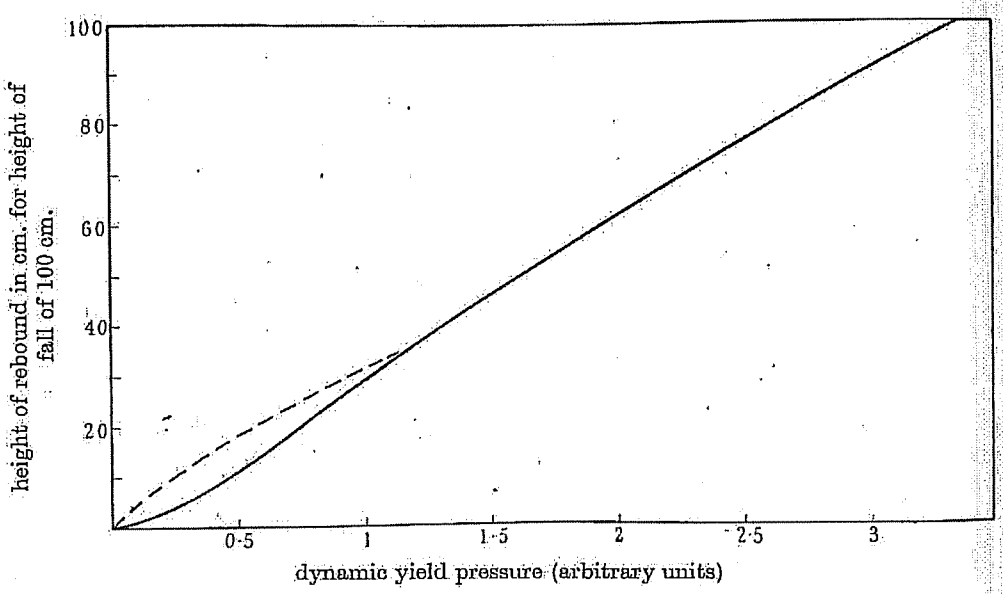

FIGURE 5

follow from this result. First, equation (12) is valid right up to a rebound of 100 %. In the latter case, the pressure obtained from equation (12) is then the final mean pressure between indenter and specimen. Secondly, plastic deformation will not occur if the yield pressure of the specimen is higher than the value of P_e given in equation (12a). As a matter of interest, it is possible to calculate the value of P_e from typical data. If the height of fall h_1 is 100 cm. and the indenter is a steel ball of mass 4 g., diameter 1 cm., and if $E_1 = E_2 = 2 \times 10^{12}$ dynes/cm.^{2}, we find that $P_e = 400$ kg./mm.^{2}. This means that if the anvil has a yield pressure* less than about

* This is the yield pressure for infinitesimal deformation. It corresponds to the transition from elastic deformation to the onset of plastic deformation and is considerably smaller than the yield pressures observed in the fully plastic deformations occurring in practical hardness

400 kg./mm.^{2} plastic flow will occur, and the height of rebound will be less than the height of fall. In this case the yield pressure of the material is given by equation (12). If, however, the yield pressure of the specimen is above 400 kg./mm.^{2}, there will be no plastic deformation of the specimen, and the height of rebound will be equal to the height of fall. In this case the rebound method will give the same height of rebound for all metals with a yield pressure higher than 400 kg./mm.^{2}. In fact, the height of rebound will be very insensitive to yield pressure above about 350 kg./mm.^{2}.

If it is wished to extend the sensitivity of the rebound method for the measurement of higher yield pressures, the experimental conditions must be modified to give a higher value for P_e in equation (12*a*). This may be readily achieved by increasing the mass of the indenter or the height of fall. For example, an increase of either of these by a factor of 32 will double the value of P_e. A more sensitive method, however, is to decrease the radius of the tip of the indenter. A decrease of r by a factor of only 3·2 will double the value of P_e. These observations may prove of value in the design of impact hardness equipment.

Coefficient of restitution

If the indenter falls with a velocity v_1 on to the surface of the anvil and rebounds with a velocity v_2, the coefficient of restitution e is defined as

$$e = v_2/v_1.$$

We may find e from equation (12) by putting $v_1^2 = 2gh_1$, $v_2^2 = 2gh_2$. Assuming that the yield pressure P remains essentially constant, equation (12) gives

$$v_2 = k(v_1^2 - \tfrac{3}{5}v_2^2)^{\frac{5}{4}}. \qquad (13)$$

It is clear from this relation that v_2 depends on v_1, so that the ratio $e = v_2/v_1$ will not be a constant. The way in which e varies with the velocity of impact is shown in figure 6, where curves i, ii, iii, iv and v respectively have been drawn for values of $e = 1$, 0·8, 0·6, 0·4 and 0·2 at an impact velocity of 450 cm./sec. (This corresponds approximately to a height of fall of 100 cm.) As will be seen later, P is not a constant, so that some deviation may be expected from these curves in practice. Nevertheless, the general form of these curves is fully confirmed in practical experiments. Typical results obtained for cast steel and drawn brass are shown in the dotted lines. Similar curves have been obtained by Raman (1918), Okubo (1922) and Andrews (1930) in experiments on the impact of spheres of similar metals. Although in this case *both* spheres are plastically deformed at the region of contact, the relation between v_1 and v_2 is of the same type as in equation (13).

measurements (see p. 264). In addition, work hardening will make this difference more marked. In a typical case Taylor (1946) finds that for a steel anvil the collisions just remain elastic when $h_1 = h_2 = 1$ cm. This corresponds to a value of P_e of about 160 kg./mm.^{2}. The steel, however, had a Brinell hardness number of 351 which means that under practical hardness measurements its yield pressure was over 360 kg./mm.^{2}.

If instead of equation (11) equation (11*a*) is used to derive the relation between v_1 and v_2, we obtain

$$v_2 = k(v_1^2 - \beta v_2^2)^{\beta}, \qquad (13a)$$

where $\beta = (2n-1)/(2n+4)$. This equation gives curves which are similar to those given by equation (13), but they are appreciably flatter.

It is apparent from these equations and from the experimental curves that in general the coefficient of restitution of impacting solids capable of undergoing plastic deformation will not be a constant. At very low velocities of impact, the pressures developed will be insufficient to cause plastic flow. The collision process will be entirely elastic and the coefficient of restitution will be unity. This occurs even with the softest metals if the velocity of impact is small enough, as Andrews (1931) showed for lead and tin alloys. As the velocity of impact increases, the amount of plastic deformation will steadily increase, and there will be a corresponding decrease in the coefficient of restitution.

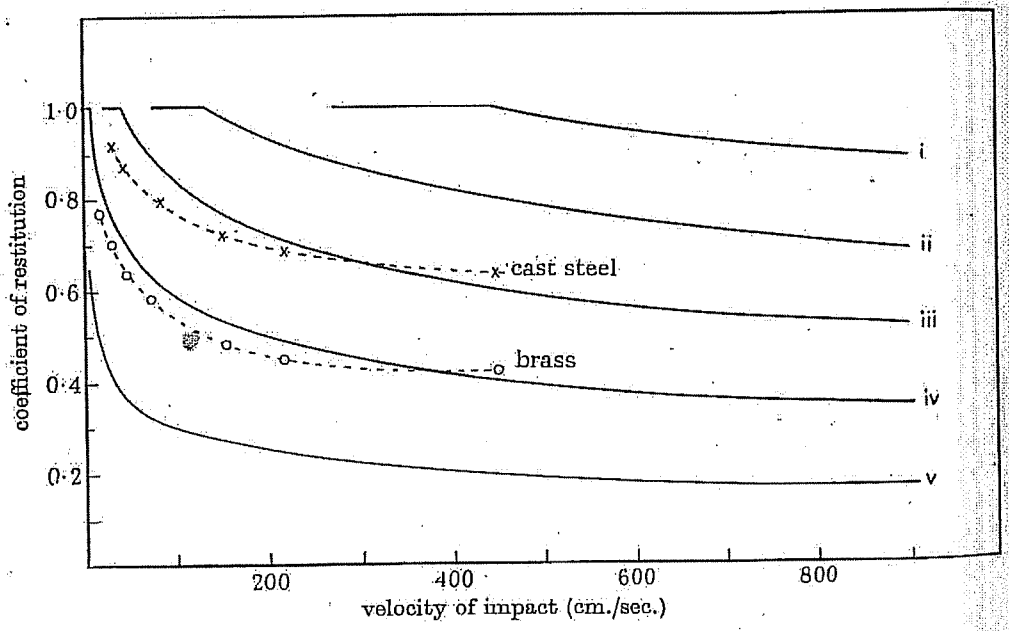

FIGURE 6

A comparison of dynamic and static hardness numbers

Some impact experiments were carried out with steel balls of diameter 0·5 and 1·0 cm. They were dropped from various heights h_1 on to massive anvils of various metals, and the height of rebound h_2 and the diameter d of the permanent indentations left in the metal surface were measured. From these observations the dynamic hardness P was calculated, using equation (11).

Some static experiments were also carried out on the same surfaces, using the same steel balls. The load L required to give an impression the same diameter as

that observed in corresponding impact experiments was found. In this way, a static yield of pressure of the material given by $L4/\pi d^2$ was calculated. We call this P_m, since it corresponds to the Meyer static hardness number. The results are given in table 6.

TABLE 6.

surface	diam. of ball (cm.)	h_1	h_2	d	$P=mg(h_1-\frac{1}{8}h_2)/V_a$ (kg./mm.²)	P_m (kg./mm.²)
hard steel	0·5	324	176	0·111	356	280
	1·0	324	176	0·133	342	290
aluminium alloy	0·5	50·4	18·5	0·057	103	80
		302	89	0·085	129	95
	1·0	50·4	20	0·113	105	81
		302	94	0·172	122	100
brass	0·5	50·5	11	0·063	74	63
		302	56	0·092	98	74
	1·0	50·5	12	0·126	73	59
		302	52	0·190	86	66
lead	0·5	51	0	0·110	8·7	5·5
		313	7·4	0·163	11·0	6·0
	1·0	51	0	0·217	9·2	5·8
		313	6·5	0·329	10·6	6·3
indium	0·5	50·6	0	0·133	4	1
		312	1·5	0·200	5	—
	1·0	50·6	0	0·266	4	—
		312	1·0	0·398	5	—

It is seen that the mean pressure required to produce plastic flow dynamically is higher than that required to produce the same amount of flow statically. This is particularly the case with the softer metals, lead and indium, and the effect becomes more marked if equation (11*a*) is used to calculate P instead of equation (11). It is also seen that the dynamic hardness is not constant but is, in general, higher the greater the height of fall h_1. This suggests that in calculating P from the volume of the indentation, part of the energy is used in the viscous displacement of the metal as the indenter sinks into the surface. This view is confirmed by a calculation of the yield pressure *from the height of rebound*. We rewrite equation (8*a*)

$$P_r^2=\frac{mgh_2}{2{\cdot}7a^3}\left[\frac{1}{1/E_1+1/E_2}\right], \tag{8b}$$

where the suffix r is added to P to show that it is calculated from the rebound height. Typical results are given in table 7.

If the last three columns are compared, it will be seen that the yield pressure P_r calculated from the height of rebound is less than the yield pressure P calculated from the volume of indentation, and somewhat greater than the static yield pressure P_m. This is what would be expected. During the formation of the indentation, when plastic flow is occurring, there is a bulk displacement of metal around the indenter.

This involves the expenditure of kinetic and viscous energy, so that the kinetic yield pressure P is appreciably higher than the static value P_m. On the other hand, at the end of the impact where the elastic compression and recovery take place, the plastic flow of the material has come to an end. There is no further bulk displacement of metal around the indenter, and no energy is expended in pushing the metal bodily away from the indentation. All the deformation around the indenter is now of an elastic nature, and any kinetic energy imparted to the material under these

TABLE 7. DYNAMIC YIELD PRESSURE P_r CALCULATED FROM HEIGHT OF REBOUND

Diameter of ball 0·5 cm. Mass 0·507 g.

	cm.			kg./mm.²		
surface	h_1	h_2	d	P_r	P	P_m
hard steel	324	176	0·111	304	356	280
brass,	50·5	11	0·063	65	74	63
$E_2 = 10 \times 10^{11}$ dynes/cm.²	302	56	0·092	82	98	74
aluminium alloy,	50·4	18·5	0·057	87	103	80
$E_2 = 7 \times 10^{11}$ dynes/cm.²	302	89	0·085	105	129	95
lead,	313	7·4	0·163	6·1	8·7	5·5
$E_2 = 1{\cdot}6 \times 10^{11}$ dynes/cm.²						
indium,	312	1·5	0·200	1·6	5	1
$E_2 = 1 \times 10^{11}$ dynes/cm.²						

conditions should be reversible. As a result the pressure at this stage may be expected to be essentially the same as P_m. This is seen to be approximately the case. For the harder metals the values of P_r are less than 10 % higher than P_m, whilst the values of P are 20 to 30 % higher. With the soft metals the difference between P and P_r becomes very marked indeed. The dynamic yield pressure P is now very much higher than the static pressure P_m, whereas P_r remains relatively close to the static values.

Discussion

These results show that when an indentation is formed in a metal surface by an impinging indenter, the pressure resisting indentation is greater than that occurring in the formation of a similar indentation under static conditions, and the higher the velocity of impact the greater the pressure of resistance. Further, the average pressure resisting indentation during the impact itself (P) is always higher than that involved at the last stages of the impact (P_r), where the plastic deformation has completely come to an end. These results are consistent with the view that the forces required to deform metals plastically are greater, the faster we attempt to deform them. This dependence of the yield pressure on the speed of deformation suggests that in the dynamic deformation of metals, forces of a quasi-viscous nature are involved.

This is borne out by the results for soft metals, lead and indium, where the pressures required to produce plastic deformation dynamically are very much greater

than the static values. This cannot be due to the work-hardening which may occur rapidly during the formation of the indentation, since at the end of the impact where the work-hardening would be a maximum, the effective yield pressure P_r is very much smaller than the mean dynamic yield pressure P which is involved during the course of the impact itself. It would seem that in the deformation of soft metals, where relatively large volumes of metal are displaced, appreciable amounts of energy are dissipated as a result of the 'viscous' flow of the deformed material surrounding the indentation.

Finally, at the end of the indentation process, where the plastic flow of the metal has come to an end and a regime of purely elastic stresses has been reached, the pressures involved (P_r) are only a few per cent higher than those involved in the formation of indentations of the same size under *static* conditions.

3. A simple theory of hardness

In this part of the paper, an attempt will be made to correlate the hardness of a metal with its elastic limit and with the way in which the elastic limit varies with the amount of deformation to which the metal has been subjected.

If p_1, p_2, p_3 are the principal stresses in a solid body, the criterion for plastic flow as proposed by Mises is that

$$(p_1-p_2)^2+(p_2-p_3)^2+(p_3-p_1)^2 = 2Y^2,$$

where Y is the elastic limit of the material as found by pure tension (of frictionless compression) experiments. The solution of Mises's equation for cases involving two-dimensional plasticity has been solved by Hencky (1923), Hill, Lee & Tupper (1947) and other workers. The solution when axial symmetry is involved presents serious theoretical difficulties which have not yet been satisfactorily resolved. Hencky has derived an approximate solution for the case of a frictionless cylindrical punch penetrating an ideally plastic solid, and finds that when plastic yielding just occurs the mean pressure on the punch P_m is about 2·8 times the yield stress Y of the material. A more rigid analysis recently carried out by Ishlinsky (1944) yields essentially the same result. Ishlinsky has also applied his analysis to the case of a frictionless spherical punch penetrating an ideally plastic solid, and finds that the mean pressure on the punch depends somewhat on the size of the indentation formed, but that to a first approximation it is equal to $2{\cdot}6Y$. This model corresponds to the Brinell indentation of a metal which does not work harden. Experiments may be carried out to test this result by using metal specimens which have been very highly worked so that they are incapable of appreciable further work-hardening. Some typical results are given in table 8, the elastic limit Y being found from careful compression experiments. The values of P_m increased slightly with the size of the impression made. It is clear, however, that to a first approximation, plastic yielding occurs when

$$P_m = cY, \tag{14}$$

where c is a constant having a value of about 3.

Now consider in somewhat greater detail the range over which equation (14) is valid. When a hard spherical indenter is pressed on to the plane surface of an ideally plastic body, the deformation of the surfaces is at first elastic and the stresses are given by Hertz's analysis. The Mises criterion indicates that the material first exceeds the elastic limit at a region below the surface of contact when the mean pressure P_m reaches a value of about $1{\cdot}1Y$ (Timoshenko 1934, p. 344). At this stage, the region of plasticity is extremely small and the permanent deformation resulting is also very small. As the load is increased the region of plasticity grows; there is a very gradual increase in the size of the indentation produced, whilst the pressure resisting deformation rises rapidly. A stage is soon reached at which the plastic region extends over the whole of the domain around the indentation. At this stage, $P_m \approx 3Y$, as given in equation (14). As we have seen, the numerical factor increases slightly with the size of the indentation, probably on account of the increased confinement of the displaced material (see Bishop, Hill & Mott 1945). This transition in the value of P_m from $1{\cdot}1Y$ to about $3Y$ is part of the intrinsic mechanism of plastic deformation and is distinct from the effects produced by work-hardening.

TABLE 8

metal	Y (kg./mm.^{2})	P_m (kg./mm.^{2})	ratio P_m/Y
tellurium lead	2·1	6·1	2·9
copper	31	88	2·8
mild steel	65	190	2·8

The onset of indentation which occurs when $P_m = 1{\cdot}1Y$ is observed only when extremely refined measurements are carried out under very small loads. Hardness measurements are usually carried out at loads well above this point, in the range where the whole of the material around the indentation flows plastically. Consequently, equation (14) may be applied to most practical hardness measurements.

Effect of work-hardening

If the metal is incapable of work-hardening, the elastic limit Y is a constant and equation (14) is valid. With most metals, however, the elastic limit depends on the amount of work-hardening which the metal has undergone, and this in turn depends on the amount of deformation to which it has been subjected. When an indentation is formed by a spherical indenter the material around the indentation will be displaced and in general the elastic limit will be raised. However, as will be seen below, the elastic limit will not be constant at every point around the indentation since the amount of deformation or strain will in general vary from point to point. We may, however, expect that there exists an average or 'representative' value of the elastic limit which is related to the mean pressure P_m by a relation of the same type as equation (14). Making this assumption a general relation between P_m and the size of the indentation may be derived.

Suppose the indentation has a diameter d and a radius of curvature r_2. Since it is a portion of a sphere its shape is completely defined by the dimensionless ratio d/r_2. Then for all indentations for which d/r_2 is the same, the amount of deformation of strain at the 'representative' region will be the same if the grain size of the material is sufficiently small as to be irrelevant. It may, therefore, be said that the strain produced at the 'representative' region is simply a function of d/r_2. Since r_2 is usually very near the radius of the indenting sphere ($r_1 = D/2$) the deformation becomes approximately equal to

$$\delta_1 = f(d/D).$$

This equation means simply that geometrically similar indentations produce similar strain distributions.

If the metal is initially fully annealed, this is the total strain produced by the indenting process. If, however, the metal has previously been cold worked, we may consider it as unworked material that has undergone an initial deformation or strain δ_0. As we shall see later, we may, to a first approximation, add this strain to that produced by the indentation. Hence the total strain δ produced at the 'representative' region of the indentation will be given by

$$\delta = \delta_0 + f(d/D).$$

We assume that the elastic limit Y is a single-valued function of the deformation or strain so that

$$Y = \phi(\delta).$$

Thus the 'representative' value of the elastic limit will be given by

$$Y = \phi(\delta_0 + f(d/D)).$$

Equilibrium is therefore set up when

$$P_m = c\phi(\delta_0 + f(d/D)), \tag{15}$$

where c is a constant having a value of about 3.

Co-ordination of results

The first result that follows from equation (15) is that we may at once co-ordinate hardness measurements made with various loads and ball diameters on a given metal specimen. For a fixed metal δ_0 is constant, so that if P_m is plotted against d/D, a smooth single-functioned curve should be obtained for all the loads and ball diameters used. Some results by Krupkowski (1931) for annealed copper are plotted in figure 7. It is seen that all the results lie about a smooth curve for ball diameters ranging from 1 to 30 mm. Further, the curve is of the same type as the elastic-limit/deformation (i.e. the stress-strain curve) for annealed copper.

Hardness as a function of the stress-strain characteristic

A more quantitative connexion between the mean pressure and the elastic limit of the material around the indentation may now be considered. A convenient method of measuring the elastic limit of a material is to determine its hardness using a

pyramidal indenter possessing a large apex angle, as in the Vicker's test. In this case, since the indentation is geometrically similar whatever its size, the mean pressure on the indenter is almost independent of the size of the indentation, i.e. the hardness is almost independent of the load. If, therefore, one measures the Vickers hardness of a metal that has been compressed or elongated by various amounts, one obtains a direct relation between the hardness number, the amount of deformation or strain and the elastic limit at any stage. This relation may then be used to determine the elastic limit of any specimen of the metal.

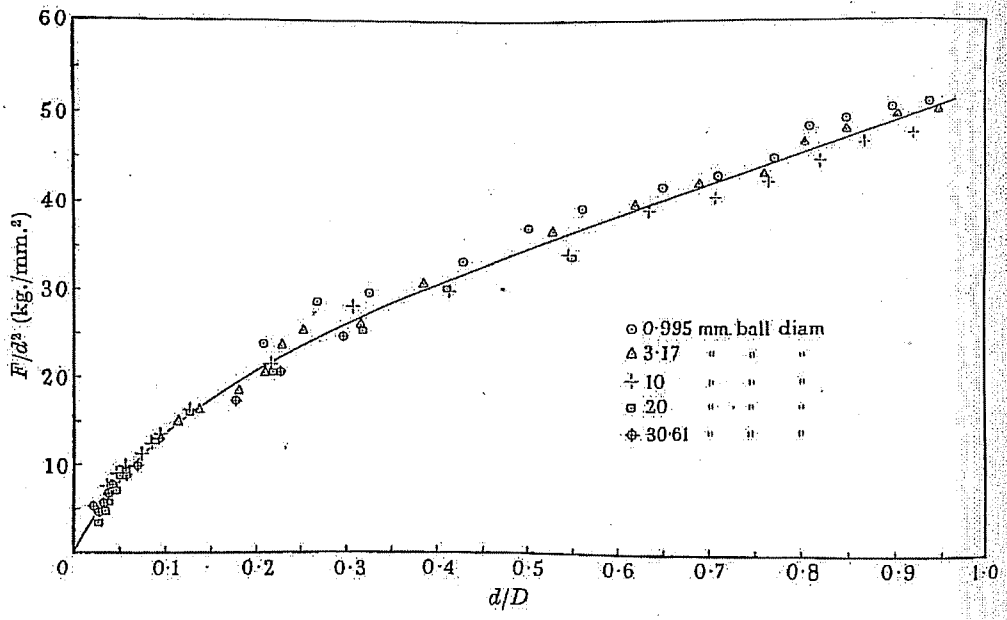

FIGURE 7

Relations of this type were determined for specimens of mild steel and annealed copper. Blocks of these metals were carefully compressed by various amounts, and the elastic limit at each stage of compression determined. The Vickers hardness numbers were also determined at each stage. Typical results for the mild steel specimens are shown in figure 8; the deformation is expressed as the change in length divided by the *compressed* length and corresponds to the fractional increase in the area of cross-section of the specimen.

Brinell impressions of various sizes were then made in the surface of mild steel and annealed copper specimens, and Vickers hardness measurements made at small loads (to give very small impressions) in the free surface of the specimen. In this way the elastic limit of the deformed material in the free surface around the indentation and in the indentation were determined. Typical results for indentations of various sizes in mild steel are shown in figure 9. It is seen that the elastic limit of the metal gradually rises as the edge of the indentation is approached. At the edge itself the elastic limit rises rapidly and then falls somewhat as the centre of the indentation is

approached. There is also a variation in elastic limit at various depths in the bulk of the material (O'Neill 1934). It would, therefore, appear difficult to assign a 'representative' value to the elastic limit of the whole material. Empirical tests

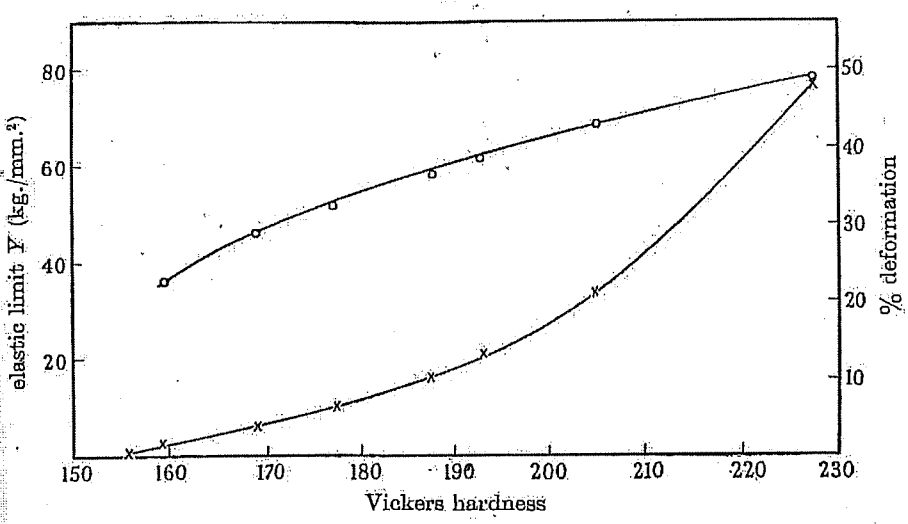

FIGURE 8. ○—○ Elastic limit. ×—× Deformation.

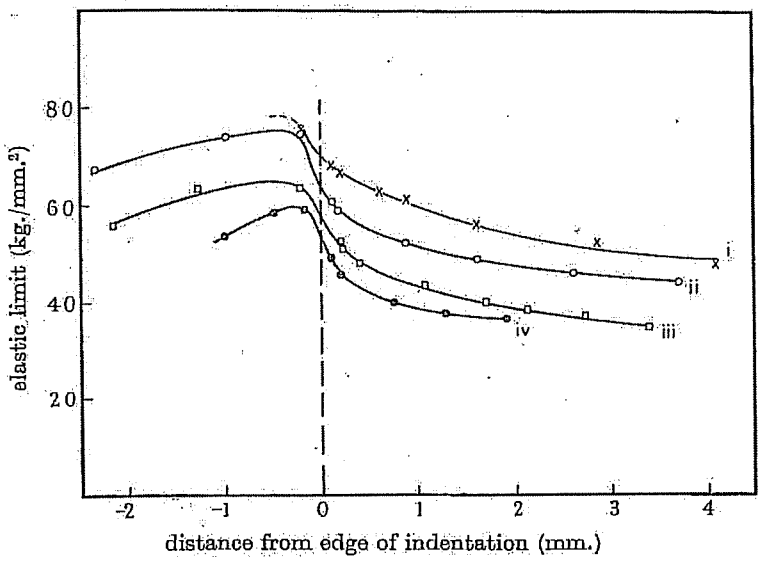

FIGURE 9. Values of d/D in curve i = 0·84, curve ii = 0·69, curve iii = 0·49 and curve iv = 0·23.

suggest, however, that the elastic limit at the edge of the indentation may be used as a 'representative' value for the whole of the deformed material around the impression. For example, we may compare the elastic limit Y_e at the edge of the indentation with the mean pressure P_m used in forming the indentation. Results

TABLE 9

metal	size of impression d/D	Y_e (kg./mm.²)	P_m (kg./mm.²)	ratio P_m/Y_e	percentage deformation corresponding to Y_e
annealed copper	0·27	10·5	27	2·6	5
	0·37	14	39	2·8	8
	0·5	16	44	2·8	9
mild steel	0·23	51	132	2·6	6
	0·49	57	159	2·7	9
	0·69	63	161	2·6	15
	0·84	70	190	2·7	~20

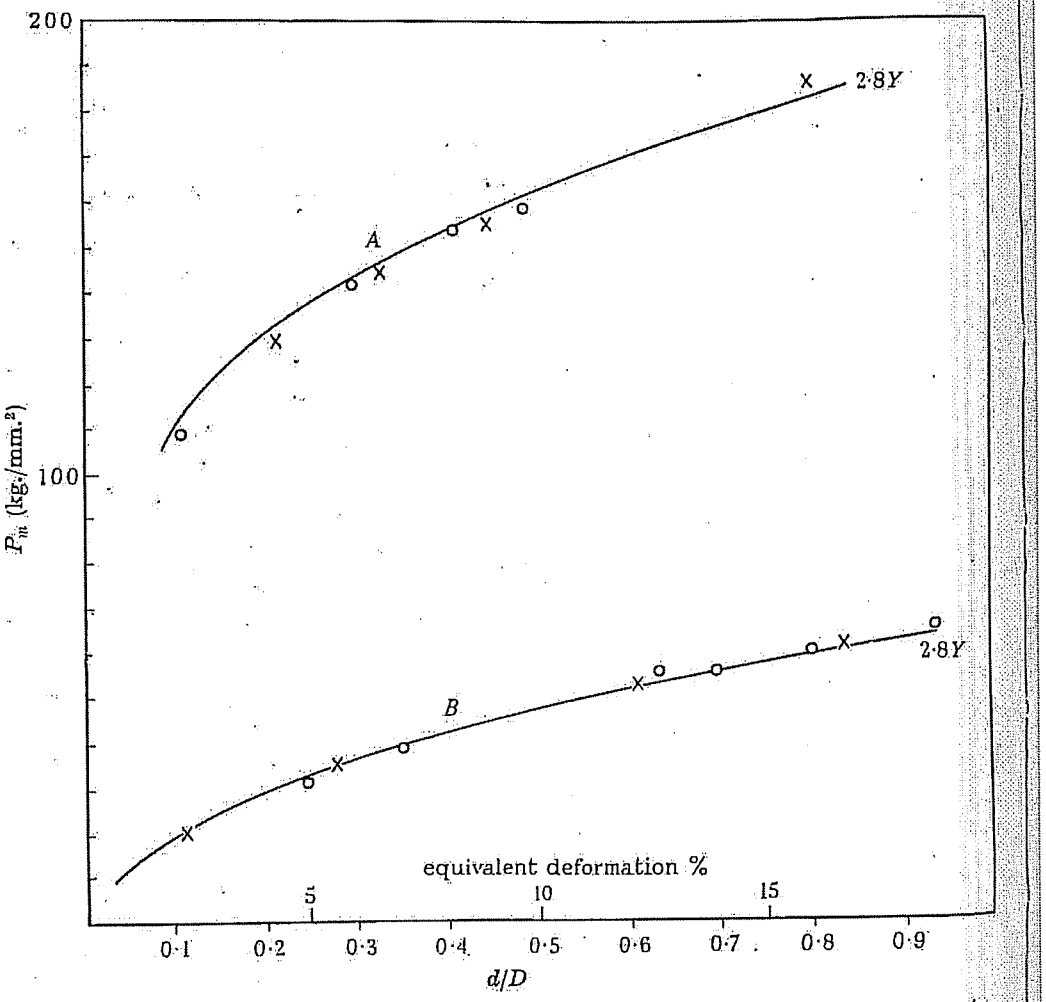

FIGURE 10. Curve *A*, mild steel. Curve *B*, annealed copper: ○ × hardness measurements. —— stress-strain curve.

for copper and steel are given in table 9. It is seen that over a wide range of indentation sizes, $P_m = cY_e$, where c has a value lying between 2·6 and 2·8. The last column of this table also shows that the deformation corresponding to Y_e is approximately proportional to the ratio d/D, i.e. if the deformation is expressed as a percentage

$$\delta_1 \approx 20d/D.$$

Similar measurements were carried out on copper and mild steel specimens that had been compressed by various amounts. It was again found that $P_m = cY_e$, where c had essentially the same value as before. It was also found that the representative deformation was approximately additive to the initial deformation, i.e. at the edge of the indentation the deformation may be written approximately as

$$\delta = \delta_0 + 20d/D.$$

Now compare the stress-strain characteristics with the hardness curves. Figure 10 shows the results obtained for annealed copper and mild steel. For the hardness curves, the values of P_m have been plotted against the values of d/D. For the stress-strain curves, the elastic limit has been multiplied by a constant factor and plotted against the deformation or strain. There is close agreement between the two curves.

The analysis may be extended to hardness measurements which have been carried out on specimens that have been deformed by various amounts. One then obtains a series of $P_m - d/D$ curves that have been displaced along the deformation axis by amounts equal to the initial deformation of the specimen. Results for annealed copper, curve B (author), and ordinary bright mild steel, curve A (author), are given in figure 11.

The hardness values for copper are for annealed specimens that have been deformed in compression experiments by 0, 9·6, 17·1, 29·6 and 41·5 %. The hardness values for mild steel are for specimens that have been deformed in compression experiments by 0, 11·4, 22·1 and 35·7 %. It is again seen that there is reasonably close agreement between the hardness curves and the stress-strain curves.*

Derivation of Meyer's laws

Meyer's laws may readily be derived from equation (15). Over an appreciable range of deformation, the elastic limit is a simple power function of the deformation or strain, i.e.

$$Y = b\delta^x, \tag{16}$$

where b and x are constants (Nadai 1931).

As we have seen, to a first approximation, the deformation δ_1 at the edge of the deformation is directly proportional to d/D. We may, however, assume a more general relation and write

$$\delta_1 = q\left(\frac{d}{D}\right)^y, \tag{17}$$

where q and y are constants.

* Similar results are obtained for metals subjected to deformation under tension. The results given by Kurth (1908) for tensile experiments on drastically annealed copper may be plotted to give a series of curves very similar to those given in figure 11.

Equation (12) then becomes

$$P_m = \frac{4F}{\pi d^2} = bc\left(\delta_0 + q\left(\frac{d}{D}\right)^y\right)^x. \tag{18}$$

For completely annealed materials $\delta_0 = 0$, so that

$$\frac{F}{d^2} = A\left(\frac{d}{D}\right)^z,$$

where $A = \frac{1}{4}\pi$, bcq = constant and $z = xy$ = constant.

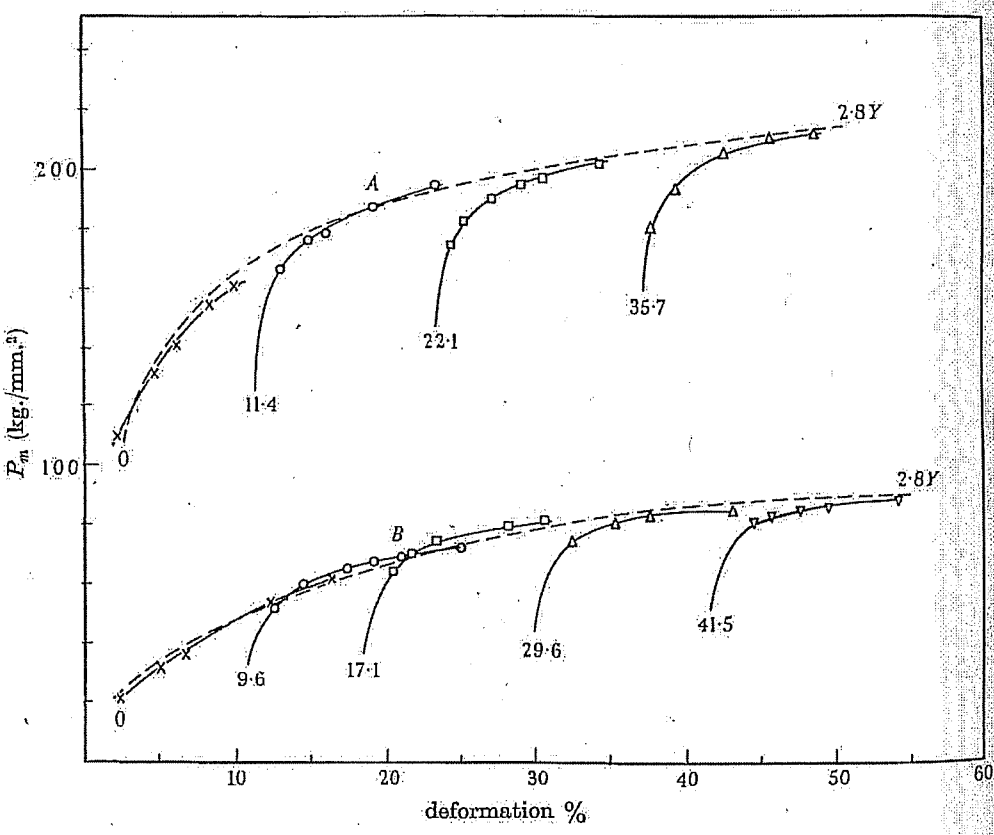

FIGURE 11. —— hardness, ––––– stress-strain. Curve A, mild steel. Curve B, annealed copper.

If for convenience we write $n = z + 2$, this yields

$$F = \frac{Ad^n}{D^{n-2}}. \tag{19}$$

Thus for indentations made with balls of different diameters D_1, D_2, D_3, ...

$$F = k_1 d^n = k_2 d^n = k_3 d^n, \tag{20}$$

where $k_1, k_2, k_3, \ldots$ are given by

$$A = k_1 D_1^{n-2} = k_2 D_2^{n-2} = k_3 D_3^{n-2}. \tag{21}$$

The two laws expressed by equations (19) and (20) (see equations (2) and (3)), were first deduced empirically by Meyer and are found to hold over a wide range of experimental conditions. Similar relations are also found to be valid for materials which have been cold-worked by various amounts.

It is interesting to note that according to the experimental measurements described above, the power y in equation (17) is approximately unity, so that n in equations (19), (20) and (21) is roughly equal to $(2+x)$. On the basis of earlier work by Kokado (1925), O'Neill (1944) has suggested that $n = 2+2x$. Most of the values given by O'Neill, however, are considerably nearer the relation $n = 2+x$, as table 10 shows.

TABLE 10. COMPARISON OF MEYER INDEX n AND STRESS-STRAIN. INDEX x. FROM DATA BY O'NEILL (1944)

metal		typical values of Meyer index n (O'Neill)	$n-2$	tensile index x	Kokado-Neill theory: $\frac{1}{2}(n-2)$
Norris data:					
mild steel A		2·25	0·25	0·259	0·12
yellow brass		2·44	0·44	0·404	0·22
yellow cold drawn		2·10	0·10	0·194	0·05
copper L		2·45	0·45	0·414	0·23
Stead data:					
steel 1A		2·25	0·25	0·24	0·12
steel 2A		2·25	0·25	0·22	0·12
steel 4A		2·25	0·25	0·19	0·12
steel 6A		2·28	0·28	0·18	0·14
Schwarz data:		(Schwarz n-values)			
brass:	annealed	2·61	0·61	0·42	0·31
	rolled	2·17	0·17	0·07	0·08
copper:	annealed	2·40	0·40	0·38	0·20
	rolled	2·12	0·12	0·04	0·06
nickel:	annealed	2·50	0·50	0·43	0·25
	rolled	2·14	0·14	0·07	0·07
aluminium:	annealed	2·20	0·20	0·15	0·10

Vickers hardness

One may expect that similar considerations will apply in the case of pyramidal and conical indenters. For these indenters the indentations are geometrically similar whatever the size of the indentation. As a result, the 'representative' deformation produced by the indentation and the 'representative' value of the elastic limit will be constant. Consequently, the mean pressure P_m required to produce plastic flow should be independent of the size of the indentation if the friction between the indenter and the metal is negligible. Experiments show that this is generally true.

In the Vickers hardness measurements a shallow pyramidal indenter is used, and the hardness number H is expressed as the ratio of the applied load to the superficial

area of the indentation formed. From the geometry of the indentation, it is found that $H = 0{\cdot}93P_m$. Empirical measurements similar to those described above suggest that the 'representative' deformation δ_1 produced by the deformation corresponds to a value of about 8 to 10 %, whilst the constant c connecting the mean pressure P_m with the 'representative' value of the elastic limit Y lies between 3·2 and 3·4.* Consequently, the Vickers hardness number is 2·9 to 3 times the 'representative' value of the elastic limit of the material around the indentation.

Typical values obtained for the steel and copper specimens used in the earlier experiments are given in table 11. Vickers hardness measurements were made on specimens of these metals after they had been deformed by various amounts δ_0. The elastic limit corresponding to a deformation of $(\delta_0 + 8)$ % was then determined from curves similar to those given in figure 9. This value is assumed to correspond to the 'representative' value of the elastic limit around the indentation. It is compared, in table 11, with the observed Vickers hardness numbers. The agreement is reasonably good over a wide range of deformations. It is also evident from the values of δ_1 and c that the Vickers hardness numbers will be close to the Brinell hardness numbers over an appreciable range of hardness values.

TABLE 11

metal	initial deformation δ_0 (%)	$\delta = (\delta_0 + 8)$ (%)	Y at δ (kg./mm.²)	cY	observed Vickers hardness number
				$2{\cdot}9Y$	
mild steel	0	8	55	159	156
	6	14	62	176	177
	10	18	66	190	187
	13	21	67	194	193
	25	33	73	211	209
				$3{\cdot}0Y$	
annealed copper	0	8	15	45	39
	6	14	20	60	58
	12·5	20·5	23·3	70	69
	17·5	25·5	25	75	76
	25	33	26·6	80	81

Discussion

The experimental results recorded in figures 10 and 11 show that there is a well-defined relation between the mean pressure P_m observed in Brinell hardness measurements and the stress-strain characteristics of the metal under consideration. In particular, the mean pressure P_m is proportional to the elastic limit Y_e of the material at the edge of the indentation. Comparison between the stress-strain curve and the

* This ratio may be compared with similar experiments described by Bishop *et al.* (1945) on the penetration of highly worked copper by hard steel cones. For a poorly lubricated cone possessing a semi-angle of 60° (this is approximately the same as that of the Vickers diamond), the pressure of penetration was 60 tons/sq.in., whilst the elastic limit of the material was 17·5 tons/sq.in. The ratio is 3·4.

hardness results show that $P_m = cY$, where c has a value of about 3. These results agree with the theoretical results of Hencky and Ishlinsky, and suggest that the elastic limit at the edge of the indentation provides a mean or representative value for the whole of the deformed material around the indentation.

The experiments also show that the elastic limit Y_e at the edge of the indentation depends on the amount of deformation produced at this region by the indentation process itself. This deformation, which is a dimensionless parameter, depends on the size of the indentation and is a function of the ratio d/D. Measurements show that the deformation is roughly proportional to d/D and that, to a rough approximation, it is additive to any work-hardening to which the metal may have been subjected in bulk.

By combining these two main results which connect P_m with Y and Y with d/D, reasonably close agreement is obtained between the hardness measurements and stress-strain characteristics of various metals. In addition, it is possible to explain the well-established empirical laws of Meyer.

The picture of the factors involved in Brinell hardness measurements, given in this part of the paper, is necessarily of a crude nature. It does not take into account the question of friction between the ball and the specimen. Nor does it tell us anything of the detailed way in which each portion of the indentation is plastically deformed and displaced. Nevertheless, it does describe the main characteristics of hardness measurements for a spherical indenter, and explains, in a semi-quantitative way, a number of well-established empirical relations. In a similar way the theory provides a semi-quantitative relation between the Vickers hardness number and the yield stress of the material.

It is clear from this analysis that hardness measurements are essentially a measure of the elastic limit of the material being examined. With pyramidal or conical indenters, where the indentation is geometrically similar whatever its size, the mean pressure to produce plastic flow is almost independent of the size of the indentation. Consequently, the hardness number has a single value over a wide range of loads. With spherical indenters, however, the amount of work-hardening and hence the elastic limit increases with the size of the indentation. As a result the yield pressure in general increases with the load. Measurements with spherical indenters thus provide information, first, about the elastic limit of the material, and secondly, about the way in which the elastic limit increases with the amount of deformation. This was first described empirically by Meyer in 1908, and the analysis given here shows that, to a first approximation, the work-hardening index x is related to the Meyer index n by the relation $x = n - 2$. In this way a series of hardness measurements with a spherical indenter may be used to determine the degree of work-hardening of a given metal.

I wish to express my sincere thanks to Mr G. Brinson of the Section of Tribophysics, Council of Scientific and Industrial Research, Australia, for carrying out a large part of the experimental work described in this paper. I should also like to thank

Professor T. M. Cherry and Dr W. Boas (Melbourne), Mr R. Hill and Dr E. Orowan (Cambridge) for valuable discussions. Finally, I wish to thank Dr F. P. Bowden for his constant encouragement, and the Ministry of Supply (Air) for a Research Grant.

References

Andrews 1930 *Phil. Mag.* **9**, 593.
Andrews 1931 *Proc. Phys. Soc.* **43**, 8.
Batson 1918 *J. Instn Mech. Engrs* **2**, 463.
Bishop, Hill & Mott 1945 *Proc. Phys. Soc.* **57**, 147.
Brinell 1900 *II. Congr. Int. Methodes d'Essai, Paris.*
Carpenter & Robertson 1936 *Metals.* Oxford University Press.
Edwards & Austin 1923 *J. Iron Steel Inst.* **107**, 324.
Foss & Brumfield 1922 *Proc. Amer. Soc. Test. Mat.* **22**, 312.
Hencky 1923 *Z. angew. Math. Mech.* **3**, 241.
Hertz 1896 *Miscellaneous papers.* London.
Hill, Lee & Tupper 1947 *Proc. Roy. Soc.* A, **188**, 273.
Ishlinsky 1944 *J. Appl. Math. Mech.* (*U.S.S.R.*) **8**, 233. English translation: Ministry of Supply A.R.D. Theoretical Research Translation, No. 2/47.
Kokado 1925 *J. Soc. Mech. Engrs Japan*, **28**, 857.
Krupkowski 1931 *Rev. Métall.* **28**, 641.
Kurth 1908 *Z. Ver. dtsch. Ing.* **52**, 1560.
Martel 1895 *Comm. des Methodes d'Essai des Materiaux de Construction.*
Meyer 1908 *Z. Ver. dtsch. Ing.* **52**, 645, 740, 835.
Nadai 1931 *Plasticity* New York.
Okubo 1922 *Sci. Rep. Tôhoku Univ.* **11**, 445.
O'Neill 1934 *The hardness of metals and its measurements.* London.
O'Neill 1944 *Proc. Instn Mech. Engrs, Lond.*, **151**, 115.
Prescott 1927 *Applied elasticity.* London.
Raman 1918 *Phys. Rev.* **12**, 442.
Shore 1918 *J. Iron Steel Inst.* **2**, 59.
Taylor 1946 *J. Instn Civil Engrs*, **26**, 486 (James Forrest Lecture).
Timoshenko 1934 *Theory of elasticity.* New York: McGraw Hill.
Vincent 1900 *Proc. Camb. Phil. Soc.* **10**, 332.